

Investigation and Implementation of MOS-FETs Losses Equations in a Three-phase Inverter

Master's thesis in Electric Power Engineering

QUE WANG

MASTER'S THESIS 2015

Investigation and Implementation of MOSFETs Losses Equations in a Three-phase Inverter

QUE WANG



CHALMERS
UNIVERSITY OF TECHNOLOGY

Department of Energy and Environment
Division of Electric Power Engineering
QUE WANG
CHALMERS UNIVERSITY OF TECHNOLOGY
Gothenburg, Sweden 2015

Investigation and Implementation of MOSFETs Losses Equations in a Three-phase
Inverter
QUE WANG

© QUE WANG, 2015.

Supervisor: Joachim Lindström, Volvo Car Group
Supervisor: Magnus Ekvall, Volvo Car Group
Examiner: Torbjörn Thiringer, Department of Energy and Environment

Master's Thesis 2015
Department of Energy and Environment
Division of Electric Power Engineering
QUE WANG
Chalmers University of Technology
SE-412 96 Gothenburg
Telephone +46 31 772 1000

Cover: MOSFET conduction losses plot during two periods.

Typeset in L^AT_EX
Printed by Chalmers University of Technology
Gothenburg, Sweden 2015

Investigation and Implementation of MOSFETs Losses Equations in a Three-phase Inverter

QUE WANG

Department of Energy and Environment

Chalmers University of Technology

Abstract

In this master thesis, the operation model of a three-phase MOSFET inverter and the corresponding current waveforms are analyzed. The mathematical expressions of the conduction losses based on the three-phase MOSFET inverter using PWM control method are presented. The algebraic equations are given with the parameters of a MOSFET-diode module, such as the on-state resistance, the body diode resistance and the voltage drop. Moreover, a numerical reference representation of the conduction losses is made to verify the analytical expressions.

Numerical analysis is firstly based on the pure sinusoidal reference three-phase voltages. The results of the numerical analysis and the results of the analytical equations are coherent. A comparison of the MOSFET inverter with reverse conduction characteristics and the assumption without reverse conduction is made. Without reverse conduction, the losses of one power module are higher than the one with reverse conduction at both the high and low current levels. The difference can be more than 20 % compared to the case with reverse condition at the rated current of the selected module, CAS300M12BM2, 150 A. When the phase current is low and there is no diode conducting during the operation, the losses without reverse conduction can be more than 100 % higher. Furthermore, the losses resulting from third harmonic injection and using the common mode reduction are calculated, and compared with the losses using a pure sinusoidal reference. The conduction losses of those two different PWM methods are found to be small and presented in tables.

Keywords: Power electronics, MOSFET, Power losses, Conduction losses, Reverse conduction, PWM, MATLAB.

Acknowledgements

This work has been carried out at Volvo Car Group and the Department of Energy and Environment at Chalmers University of Technology. The author would like to thank her supervisors at Volvo Car Group, Joachim Lindström and Magnus Ekvall, as well as her examiner at Chalmers, Torbjörn Thiringer, for their never-ending support and valuable advice. The author would also like to thank the Division of Electric Power Engineering for the support of software and hardware when she was writing the academic report.

QUE WANG, Gothenburg, August 2015

Nomenclature and Abbreviations

Symbol	Quantity	Unit
V_A	Potential of phase A	V
V_B	Potential of phase B	V
V_C	Potential of phase C	V
V_{DC}	DC link voltage	V
u_{inst}	Instantaneous voltage of one phase	V
d	Duty cycle	-
M	Modulation index	-
i	Instantaneous current	A
p_{diode}	Instantaneous power losses of the diode	W
v	Instantaneous voltage	V
i	Instantaneous current	A
i_{rms}	Root mean square value of the current in the component	A
i_{avg}	Average value of the current	A
P_{diode}	Average power losses of the diode	W
t	Time	ms
T	Fundamental period	ms
p_{IGBT}	Instantaneous power losses of the IGBT	W
P_{IGBT}	Average power losses of the IGBT	W
R_F	Equivalent resistance of the IGBT	Ω
V_T	Equivalent voltage drop of the IGBT	V
p_{MOSFET}	Instantaneous power losses of the MOSFET	W
P_{MOSFET}	Average power losses of the di MOSFET ode	W
α	Displacement power factor angle	radians
β	Turn-on(conduction) angle	radians
R_{on}	Equivalent resistance of the MOSFET	Ω
R_d	Equivalent resistance of the diode	Ω
V_d	Equivalent voltage drop of the diode	V
\hat{I}	Peak value of the phase current	A
I_{rms}	Root mean square value of the phase current	A
f_{sw}	Switching frequency	Hz
f_1	Fundamental frequency	Hz
\hat{U}	Peak value of the phase voltage	V

Abbreviation	Explanation
HEV	Hybrid electric vehicles
DC	Direct current
AC	Alternating current
SiC	Silicon carbide
MOSFET	Metal-oxide-semiconductor Field-effect Transistor
IGBT	Insulated-gate Bipolar Transistor
PWM	Pulse Width Modulation
SPWM	Sine-triangle pulse width modulation
RMS	Root mean square
AVG	Average
THIPWM	Third Harmonic Injection Pulse Width Modulation

Contents

Abstract	vi
Acknowledgements	viii
Nomenclature and Abbreviations	ix
1 Introduction	1
1.1 Background of power losses in inverters	1
1.2 Purpose of the thesis	2
1.3 Methods	2
2 Theory of a Three-phase Inverter	5
2.1 Introduction of a three-phase inverter	5
2.1.1 PWM control method in a three-phase inverter	5
2.1.2 Operation model during different time interval in one switching period	8
2.2 Introduction of semiconductor switches: MOSFET, IGBT and diode .	11
2.2.1 Functionalities of MOSFET, IGBT and diode	11
2.2.2 Basic losses-equations of diode, IGBT and MOSFET	16
3 Operation Model of a Three-phase MOSFET Inverter Using PWM	17
3.1 Three-phase MOSFET inverter system with reverse conduction MOSFET	17
3.1.1 The structure of a three-phase MOSFET inverter	17
3.1.2 The structure of one leg of the three-phase MOSFET inverter	17
3.2 The current flow in one leg of a three-phase MOSFET inverter	19
3.2.1 Current waveforms of pure MOSFET conduction during low current flow in the system	19
3.2.2 Current waveforms of both MOSFET and diode conduction during high current flow in the system	20
3.3 Current analysis in the reverse conductive MOSFET	22
4 Conduction Losses Calculation and Analysis	25
4.1 MOSFET conduction losses	25
4.2 Diode conduction losses	26
4.3 Equations of conduction power losses during different time interval .	26
4.3.1 The expressions of MOSFET conduction losses in one period .	27

4.3.2	The expressions of diode conduction losses in one period	28
4.3.3	Boundary condition when the diode starts conducting	28
4.4	Total Conduction losses equations during one period	29
5	Verification Using Numerical Analysis	31
5.1	Prerequisites of the numerical analysis	31
5.2	Numerical losses calculation	32
5.2.1	Calculation procedure	32
5.2.2	Results of the numerical reference system and verification with theoretical calculation	34
6	Theoretical Analysis and Comparison between MOSFET with re- verse conduction and without reverse conduction	37
6.1	Theoretical analysis of the mathematical equations with MOSFET reverse conduction	37
6.2	Comparison and analysis between MOSFET with reverse conduction and without reverse conduction	39
7	Conduction Losses Calculation using two different PWM Methods	43
7.1	Numerical results with the third harmonic injection	43
7.1.1	Reference voltage design principle	43
7.1.2	Results and comparison	43
7.2	Results with the common mode reduction	45
7.2.1	Voltage design principle	45
7.2.2	Results and comparison	46
8	Conclusion	49
9	Future Work	51
	Bibliography	54
10	Appendix 1	55

1

Introduction

Currently, with the development of the worldwide automotive industry and the increase of the world population, the demand of vehicles for personal transportation has increased dramatically, especially in China, India and some developing countries [1]. Moreover, the environmental awareness, continuous oil price increase and national or European environmental ambitious such as the 20-20-20 target [2], have increased the importance of the research on electrification of vehicles more and more. Thus, the analysis of power losses in the advanced vehicular power system needs more effort to contribute to the development of the automotive world. In this chapter, some background of power losses in inverters, the purpose of the thesis and investigation methods will be introduced.

1.1 Background of power losses in inverters

With more regulations and constraints on the energy resources, hybrid and electric cars are attracting attention by automakers, governments, and customers [3]. The demands for improved fuel economy and more electric power are driving advanced vehicular power system voltages to higher levels. Since hybrid electric vehicles (HEV) are likely to dominate the advanced propulsion in coming years, the hybrid technology becomes significant. Furthermore, power electronic devices such as DC to AC inverters are inherent parts of electrified vehicles. Moreover, in the design of the powertrain components, power electronics converters are shown to be one of the most challenging parts presented in advanced propulsion systems. Besides, in battery chargers and a class of DC and AC motor drives, the application of power electronic converters with controllable switches is quite necessary. Therefore, significant amount of research has been conducted on three-phase inverters.

In today's propulsion systems of hybrid cars, it is common to use IGBT inverters operating according to the PWM principle. The losses equations of the IGBT inverters have been solved and can be used for the calculation [4]. Based on the comparisons of the MOSFET and IGBT inverters in the motor drive systems in the literature, the SiC MOSFET inverters have the advantages of lower losses, better efficiency and smaller size in the same motor drive application [5]. Due to the possible reverse conduction opportunities of MOSFETs, the equations of the IGBTs in [4] are insufficient to be used for calculating the conduction losses of the MOSFET inverters. Thus, it is significant to derive the conduction losses equations of the

MOSFET inverters, so they can be used for future calculations. According to the author's search, the conduction losses equations of the MOSFET inverters have not been found in available publications. For future use, the equations of power losses in MOSFET inverters need to be derived.

1.2 Purpose of the thesis

The main objective of the work reported in this thesis is to derive the mathematical expression of the conduction losses in a three phase MOSFET inverter. With the equations, the inverter power losses under various DC voltages, various phase currents, various modulation indices, and various basic parameters based on the physical structures of the inverters, can be calculated instantaneously by the softwares, for instance, MATLAB. The results presented in this thesis are from an analytical model as well as from a numerical reference model.

1.3 Methods

In order to be able to calculate the power losses in MOSFET inverters, it is vital to have a good understanding of the components functionalities, and the on-state characteristics. Equivalent circuits will be investigated when each component is conducting.

Once the relation is known, the current waveforms of different components can be produced in detail. The conduction losses equations are given from [6]. Thus, the equations in one leg of the three-phase MOSFET inverter can be derived, both for the MOSFET and the diode.

The following task is to derive the conduction power losses equations mathematically. Thus, the algebraic formulas are necessary to be used. The final conduction losses expressions will be implemented in MATLAB for further use.

After the investigation of the losses equations, the numerical calculations will be presented. This part is done using MATLAB. The conduction losses will be shown in tables and will be verified with the analytical results utilizing the selected component.

Moreover, the comparison of the MOSFET inverter with reverse conduction characteristics and the assumption without reverse conduction is made. The loss calculation are performed at both the high and low current levels. The differences are shown in tables.

The last task is to investigate the conduction power losses in realistic inverter designs, using third harmonic injection and the common mode reduction, using the results from the previous tasks. The deviations will be presented and compared to pure sinusoidal reference voltages.

2

Theory of a Three-phase Inverter

In this chapter, the theory of a three-phase inverter will be presented. First, the topology of a three-phase inverter will be shown and the explanation of the operation principle and performance will be given. Secondly, the functionalities and basic power losses equations of the semiconductor switches will be introduced.

2.1 Introduction of a three-phase inverter

The topology of a three-phase inverter is shown in Figure 2.1. The inverter consists of three phase legs, each leg includes two non-reverse conduction switches in either the up or down position. There is a diode in anti-parallel with each corresponding switch, which is used to provide a path for a current flowing in the opposite direction. It always occurs due to the loads are inductive. For example, if the load current is negative at the instant when the upper transistor is gated on, the diode in parallel with the upper transistor will conduct until the load current becomes positive, and at that time the upper transistor will begin to conduct. There is a capacitor on the DC side, which is assumed to supply a stiff DC voltage in this analytical model. And the loads of the system are modeled with large inductors, which give the continuous currents following the reference current waveforms. The inductive loads with a back emf represent the electric machine in an electric drive system. There is a 120° shift between each phase.

2.1.1 PWM control method in a three-phase inverter

One of the widely used inverter control methods covered in power electronics is the sine-triangle pulse width modulation (SPWM) control. With the SPWM control method, the switches of the inverter are controlled based on a comparison of sinusoidal control reference signals and a triangular carrier wave [7]. The sinusoidal control waveform establishes the fundamental frequency of the inverter output, while the triangular waveform presents the switching frequency of the inverter. The ratio between the frequencies of the sinusoidal reference wave and the triangular wave is referred to as the modulation frequency ratio [8].

The switches in each leg of a three-phase inverter are never both on or off simultaneously; therefore, the potentials V_A , V_B , and V_C alternate between the input voltage

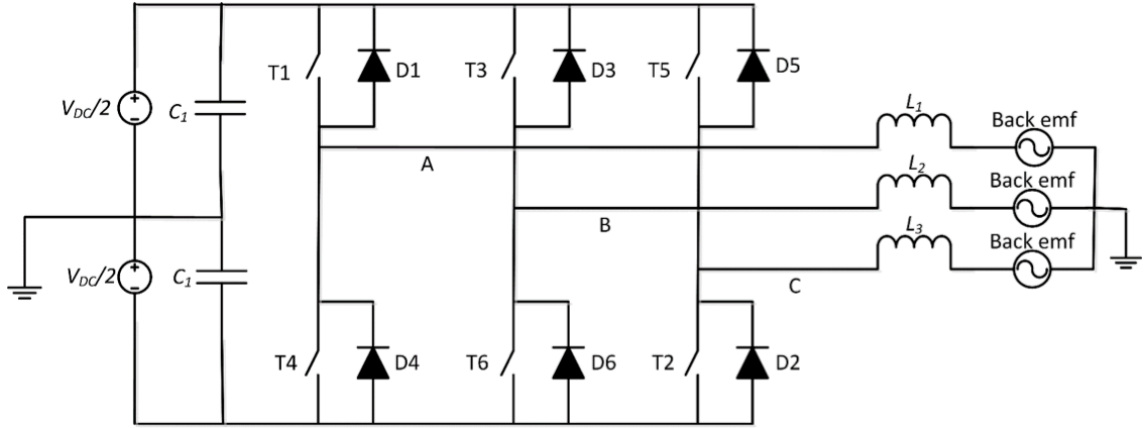


Figure 2.1: The structure of a three-phase inverter with non-reverse conduction switches, an associated DC link capacitor and inductive loads.

(V_{DC}) and zero. Using this method, the phase potentials are AC, with a fundamental frequency corresponding to the frequency of the sinusoidal reference signals. The magnitude of the triangle wave is fixed. Thus, the amplitude of the output potential is controlled by adjusting the amplitude of the sinusoidal reference signals. [8]

Based on the research in [9], using the PWM modulation method, the instantaneous duty cycle can be written as

$$d(t) = \frac{1}{2}(1 + M \sin t) \quad (2.1)$$

for a pure sinusoidal wave. In (2.1), d is the duty cycle of one leg. M is the modulation index of the PWM control method, which is between 0 and 1. The time intervals when the upper semiconductors are conducting can be calculated from (2.1). Consequently, $(1-d)$ gives the time intervals when the lower semiconductors are conducting. [9]

The output potential of one phase is shown in Figure 2.2 using SPWM in the one-leg model. The DC link voltage is 400 V in this case, which can be utilized in the electric drive system of a hybrid car. The switching frequency of the theoretical model in this case is 2 kHz, which is suitable for the analysis of the waveforms. The black curve in Figure 2.2 represents the triangle wave, the magenta curve, u_1 , is the reference signal of one phase, the blue curve, u_{1inst} , shows the instantaneous voltage of the phase, and the red line, $u_1(time)$, is the fundamental output potential of the phase. Therefore, the corresponding phase current waveform can be drawn as in the following section. Since all of the three phases in the inverter have a 120° shift between the other two phases, it is enough to analyze the operation principle using one leg of the three-phase inverter. There is an impact due to the natural point will not be zero all the time in the three-phase inverter, but it will not influence the coming visualizations. Thus, the total losses in a three-phase inverter will be three times of the losses in one leg. For the analysis part, the one-leg topology will be

introduced.

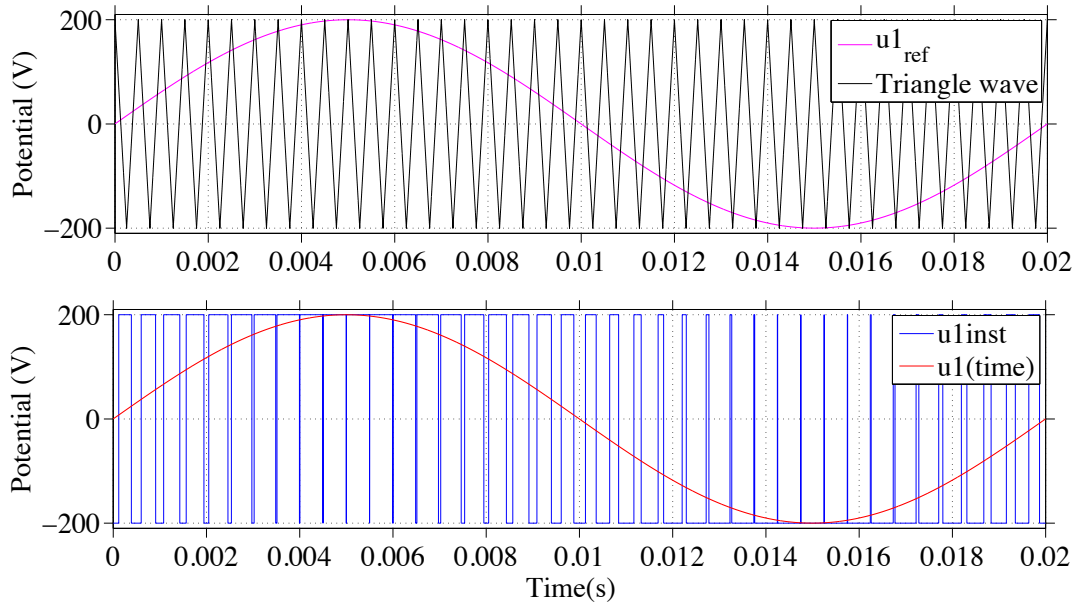


Figure 2.2: The potential waveforms over one switch during one period using PWM. The upper one shows the triangular wave and the sinusoidal reference signal of one phase, $u1$. The lower one shows the instantaneous phase potential, $u1_{inst}$, and the fundamental output potential, $u1(time)$.

2.1.2 Operation model during different time interval in one switching period

Figure 2.3 shows a one-leg topology of a three-phase inverter with general controllable switches. The one-leg topology contains T1 and D1 in the upper part and T4 and D4 in the lower part. A DC voltage (V_{DC}) and an inductive load are utilized in the description. Each of the switches and diodes in Figure 2.3 are drawn in different colours to facilitate in the upcoming analysis regarding the current waveforms.

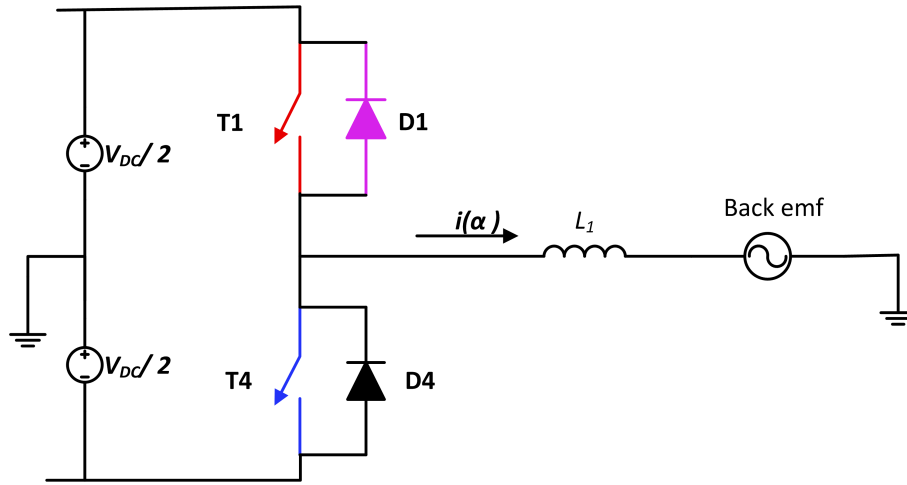


Figure 2.3: One leg of the three-phase inverter with back emf.

The corresponding phase current waveforms in one diode-switch combination during one period using PWM are reached under $u1(time)$ of Figure 2.2. Since the system includes inductive loads, thus, the output current is often lagging, which can be expressed as

$$i(t) = \hat{I} \sin(\omega t - \varphi), \quad (2.2)$$

where φ is the angle difference between the fundamental phase potential and the current waveform. In Figure 2.4, the current through the upper switch and diode is shown. The dashed line, i_1 , is the phase current with I_{rms} being 375 A, which is high enough and can be used in the hybrid system with the IGBT inverter. In this figure, a phase shift is shown. The red curve, i_{T1U} , represents the current through the switch, and the magenta, i_{D1U} , curve provides the current through the corresponding diode.

Correspondingly, the current through the lower switch and diode is presented in Figure 2.5. The blue curve, i_{T1L} , represents the current through the lower switch, and the black curve, i_{D1L} , is the current through the corresponding diode. From those two figures, it can be seen that the upper switch and lower diode take up the whole positive load current shape, and the lower switch and the upper diode take up the negative half period.

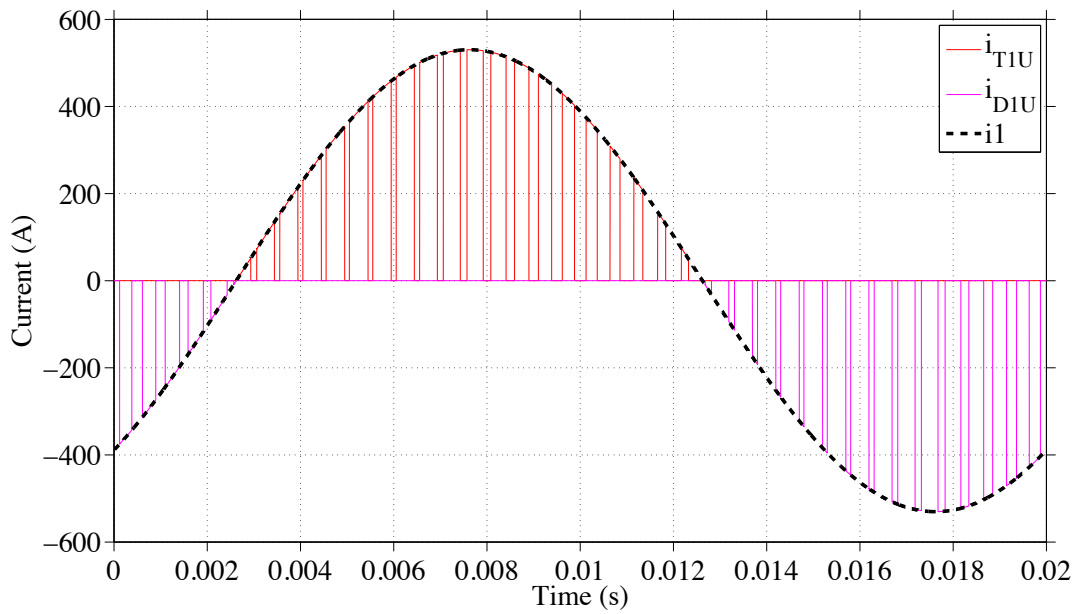


Figure 2.4: The current waveform in upper diode and switch during one period using PWM. The dashed line is the phase current, i_1 , the red curve represents the current through the upper switch, i_{T1U} , and the magenta curve is the current through the corresponding diode, i_{D1U} .

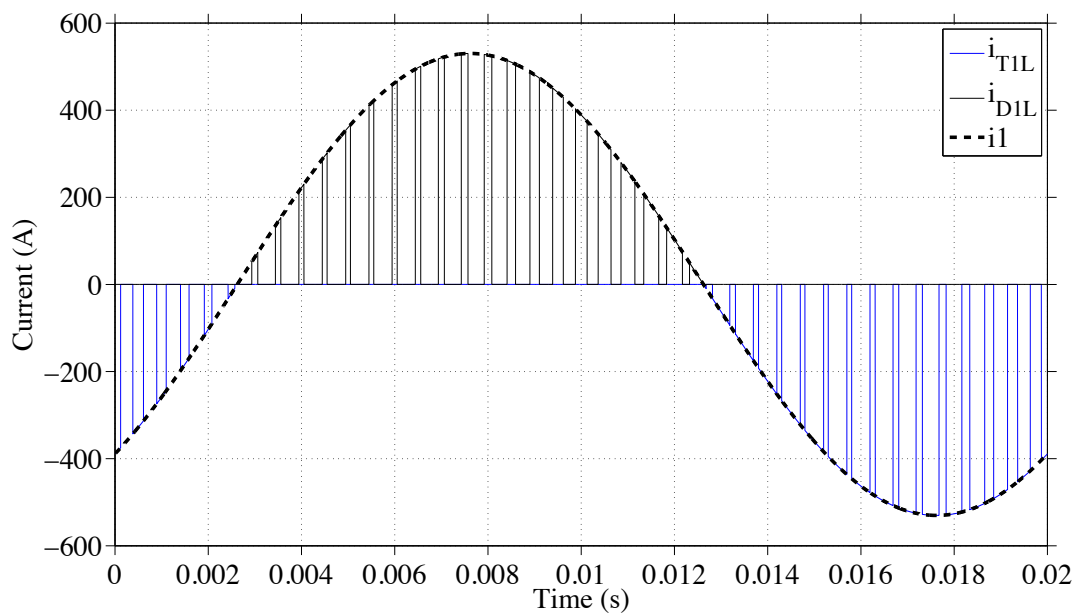


Figure 2.5: The current waveform in lower diode and switch during one period using PWM. The dashed line, i_1 , is the phase current, the blue curve, i_{T1L} , represents the current through the lower switch, and the black curve, i_{D1L} , is the current through the corresponding diode.

2.2 Introduction of semiconductor switches: MOSFET, IGBT and diode

2.2.1 Functionalities of MOSFET, IGBT and diode

Each component in a three-phase inverter has a unique functionality, which is why different forms of equations are used in the losses calculation. Thus, the characteristics of each component need to be introduced in this section.

Firstly, the symbol and the steady-state i - v characteristic of a diode are shown in Figure 2.6 [6]. When the diode is forward biased, it begins to conduct with a small forward voltage across it. Thus, the characteristics can be simplified as shown in Figure 2.7. In the analysis of the inverter topology, the on-state condition of the diode can be represented by a resistor in series with a voltage source.

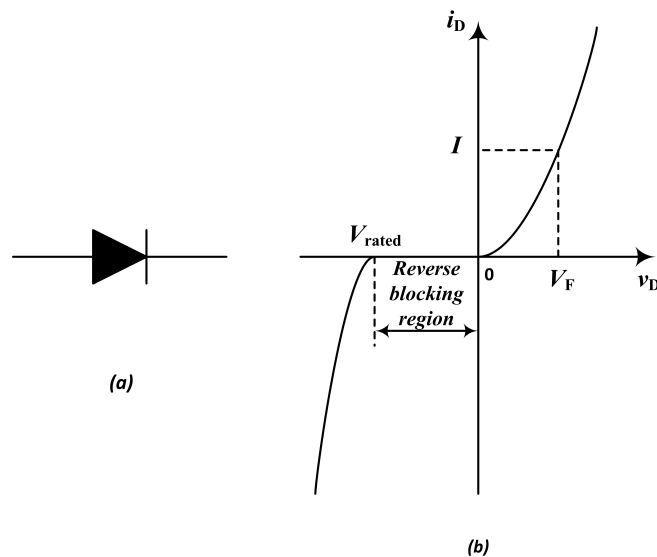


Figure 2.6: Diode: (a) symbol, (b) i - v characteristic.

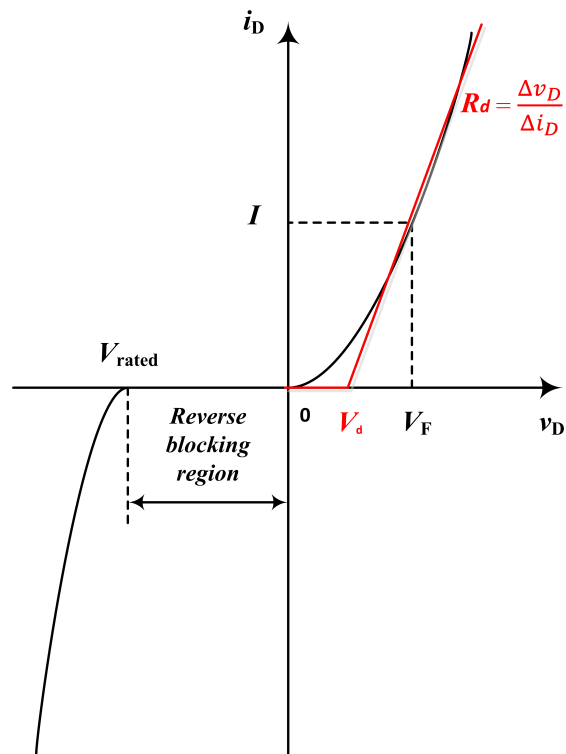


Figure 2.7: Simplified characteristics of the diode. The red curve shows the relation between the voltage and the current, and the linearized line gives the equivalent resistance of the diode and the small voltage drop, V_d .

Secondly, Figure 2.8 shows the symbol for an IGBT to the left and its i - v characteristics to the right [6]. Similar to a diode, the simplification of the IGBT characteristics can be drawn as it is shown in Figure 2.9. The equivalent model of an IGBT can be drawn as a resistance, R_f , and a voltage drop, V_T , in series.

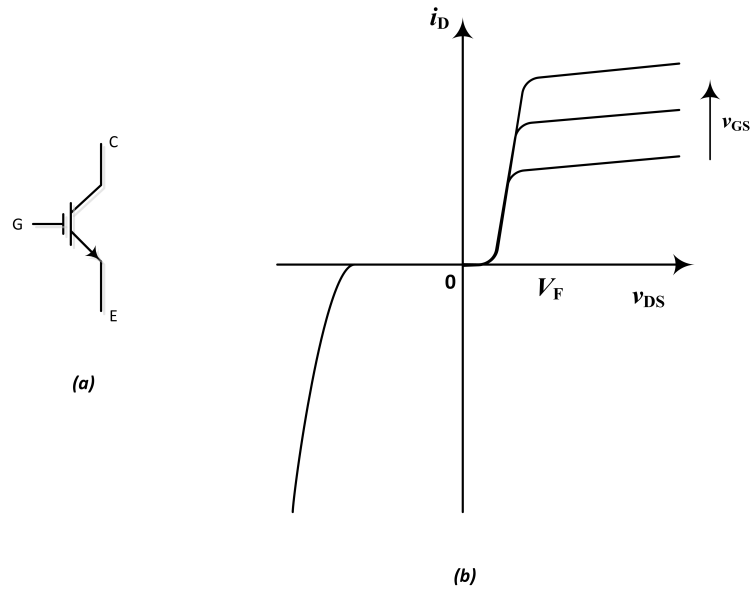


Figure 2.8: An IGBT: (a) symbol, (b) i - v characteristic.

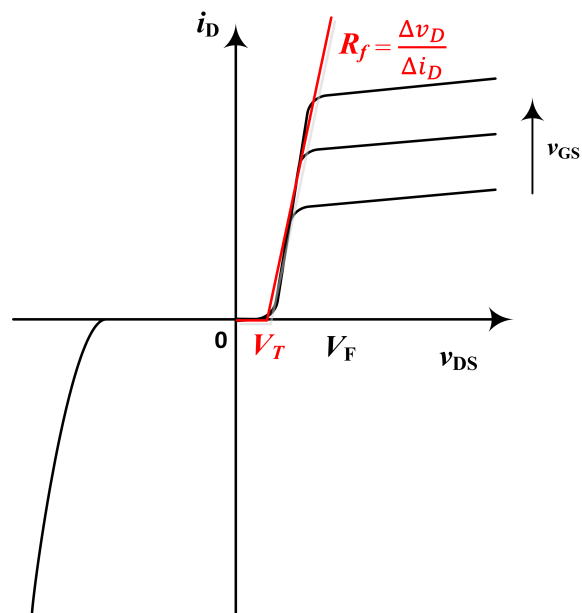


Figure 2.9: Simplified characteristics of the IGBT. The red curve shows the relation between the voltage and the current, and the linearized line gives the equivalent resistance of the IGBT, R_f , and the small voltage drop, V_T .

The circuit symbol of an n-channel MOSFET is shown in Figure 2.10 (a). The i - v characteristics are shown in Figure 2.10 (b). The differences are shown in Figure 2.10 (b), when V_{GS} is high enough, the current increases while the voltage increases, and there is no constant voltage-drop term. Then the simplified characteristics can be drawn in Figure 2.11. Therefore, the equivalent circuit of an on-state MOSFET can be drawn as a resistor, R_{on} [6].

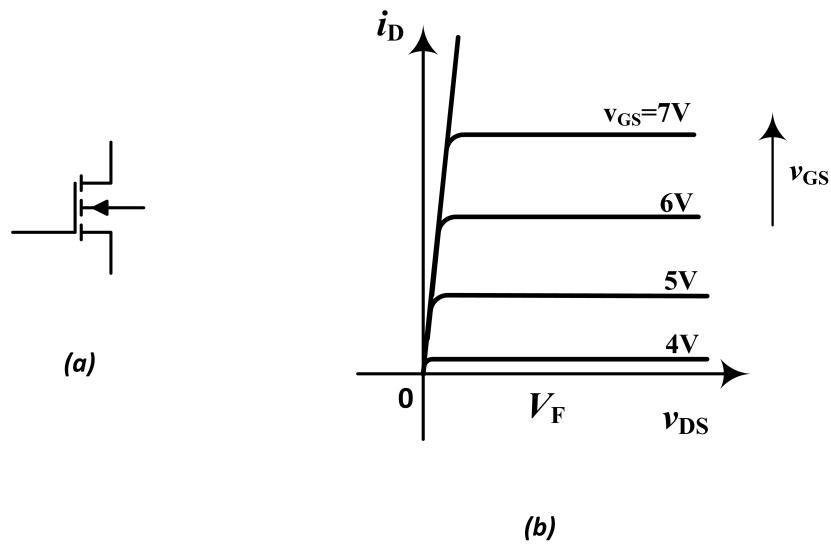


Figure 2.10: N-channel MOSFET: (a) symbol, (b) i - v characteristic.

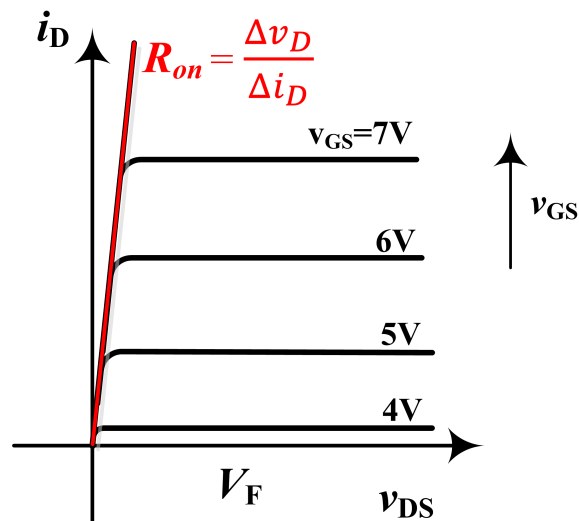


Figure 2.11: Simplified characteristics of the MOSFET. The linearized curve shows the equivalent resistance of the MOSFET, R_{on} .

2.2.2 Basic losses-equations of diode, IGBT and MOSFET

The on-state losses-equations of the diode can be written as

$$p_{diode}(t) = v(i(t))i(t) = (R_d i(t) + V_d)i(t) = R_d i^2(t) + V_d i(t), \quad (2.3)$$

$$\begin{aligned} P_{diode} &= \frac{1}{T} \int_0^T v(i(t))i(t) dt \\ &= \frac{1}{T} \int_0^T (R_d i(t) + V_d)i(t) dt \\ &= \frac{1}{T} \int_0^T (R_d i^2(t) + V_d i(t)) dt \\ &= R_d i_{rms}^2 + V_d i_{avg}, \end{aligned} \quad (2.4)$$

where p_{diode} is the instantaneous power losses of the diode, and P_{diode} is the average power losses of the diode during one fundamental period. i_{rms} is the root mean square(RMS) value of the current and i_{avg} is the average value of the current. T is the fundamental period.

$$p_{IGBT}(t) = v(i(t))i(t) = (R_f i(t) + V_T)i(t) = R_f i^2(t) + V_T i(t), \quad (2.5)$$

Similarly, the on-state power losses equations of the IGBT can be written as

$$\begin{aligned} P_{IGBT} &= \frac{1}{T} \int_0^T v(i(t))i(t) dt \\ &= \frac{1}{T} \int_0^T (R_f i(t) + V_T)i(t) dt \\ &= \frac{1}{T} \int_0^T (R_f i^2(t) + V_T i(t)) dt \\ &= R_f i_{rms}^2 + V_T i_{avg}, \end{aligned} \quad (2.6)$$

where p_{diode} is the instantaneous power losses of the diode, and P_{diode} is the average power losses of the diode during one fundamental period.

$$p_{MOSFET}(t) = v(i(t))i(t) = R_{on} i^2(t) \quad (2.7)$$

$$\begin{aligned} P_{MOSFET} &= \frac{1}{T} \int_0^T v(i(t))i(t) dt \\ &= \frac{1}{T} \int_0^T R_{on} i^2(t) dt \\ &= R_{on} i_{rms}^2 \end{aligned} \quad (2.8)$$

The power losses equations of the MOSFET are given in (2.7) and (2.8), where p_{MOSFET} is the instantaneous power losses of the MOSFET, and P_{MOSFET} is the average power losses of the MOSFET during one fundamental period. It can be seen in those equations that there is no constant voltage-drop term in the losses calculation.

3

Operation Model of a Three-phase MOSFET Inverter Using PWM

In this chapter, the investigation is focused on using MOSFETs as the switches instead of IGBTs. The MOSFET inverter is analyzed in detail. This part is conducted based on one leg of the three-phase inverter. Current waveforms are shown both at the high amplitude level and at the low amplitude level.

3.1 Three-phase MOSFET inverter system with reverse conduction MOSFET

3.1.1 The structure of a three-phase MOSFET inverter

Figure 3.1 shows the topology of a three-phase MOSFET inverter. All of the switches are n-channel MOSFETs in this case. For the analytical model, the capacitor on the DC side is assumed to be large enough to provide a stiff voltage. The inverter has a large inductive load which gives a continuous current. As it is mentioned in Chapter 2, due to the 120 ° shift principle, all of the three phases carry the same shape of the currents during one period, therefore, it is enough to analyse only one leg of the three-phase inverter to derive the losses equations. Then the total losses in the inverter will be three times of the losses of one leg. Thus, in the following sections, the one-leg topology will be analyzed in detail.

3.1.2 The structure of one leg of the three-phase MOSFET inverter

In Figure 3.2, the one-leg topology of a three-phase inverter is shown, which will in principle give the same results as one leg of the three-phase MOSFET inverter. The upper MOSFET, M1, is marked in red, and the lower MOSFET, M4, is drawn in blue. Meanwhile, the upper diode, D1, is presented in magenta, and the lower diode, D4, is in black. In the following analysis of current flow, the current curves will be shown using the corresponding colours.

Since during one period, each time point can correspond to a certain phase angle,

3. Operation Model of a Three-phase MOSFET Inverter Using PWM

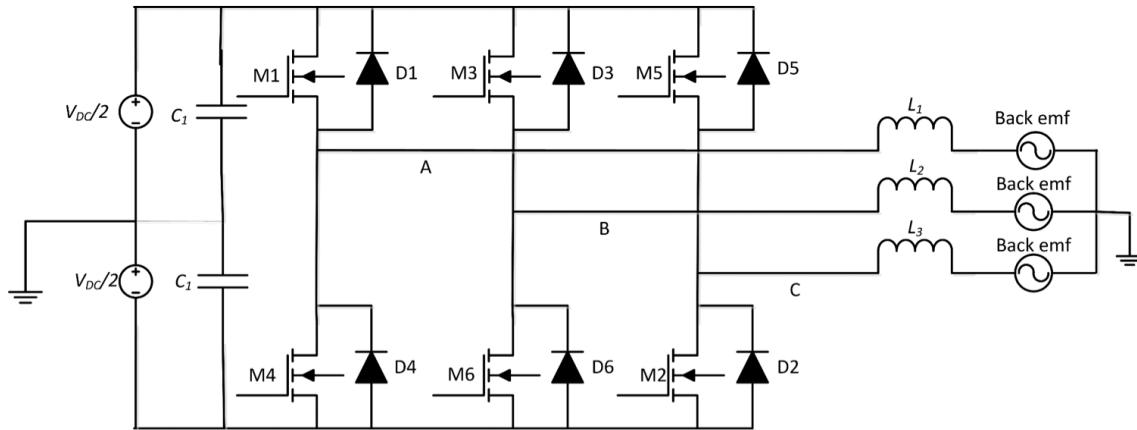


Figure 3.1: The structure of a three-phase MOSFETs inverter with large capacitor and large inductive loads.

which can be expressed as

$$\alpha = \frac{2\pi}{T}t, \quad (3.1)$$

thus, the output current is marked as $i(\alpha)$ in Figure 3.2. From the same method, all calculations are based on the angle in the following analysis of the current flow and power losses.

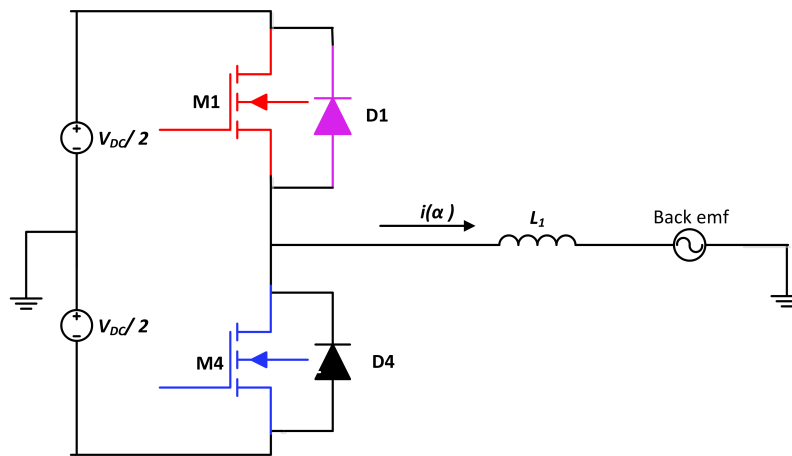


Figure 3.2: The topology of one leg of a three-phase MOSFETs inverter with an inductive load.

3.2 The current flow in one leg of a three-phase MOSFET inverter

In the following analysis, the circuit in Figure 3.2 is chosen to be the model when the currents are simulated. Unless stated in this chapter, 2 kHz will be used as the switching frequency. All the currents in the MOSFETs and diodes are shown as the absolute values in the figures in this section.

3.2.1 Current waveforms of pure MOSFET conduction during low current flow in the system

Using the one-leg topology analysis, the current flows of the leg can be shown in Figure 3.3, Figure 3.4 and Figure 3.5 for one fundamental period. In this case, in order to have no current in the diode, the RMS value of the load phase current is selected to be 20 A. It can be seen from Figure 3.3 and Figure 3.4, if the amplitude of the phase current is not high enough, only the MOSFETs are conducting. Figure 3.5 shows that during one period, the phase current is the sum of the currents through the upper MOSFET and the lower MOSFET.

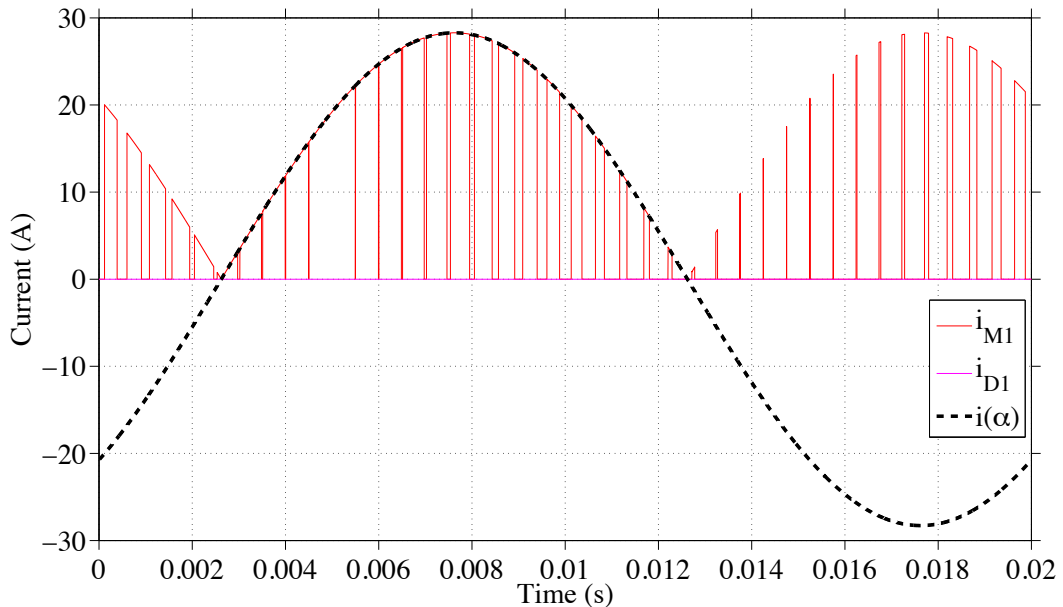


Figure 3.3: The currents through M1 and D1 and the phase current $i(\alpha)$ during one period.

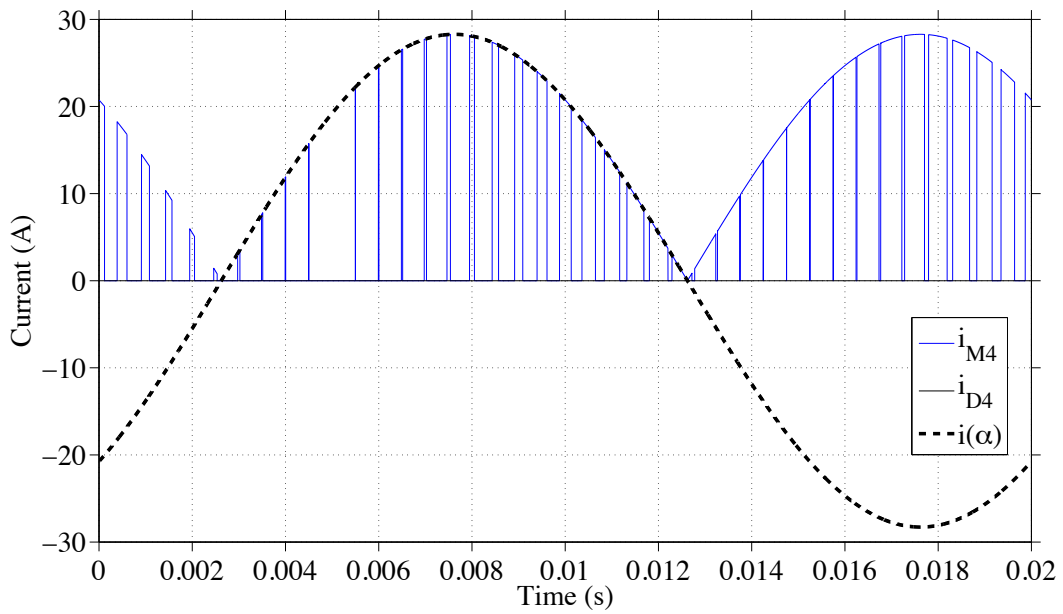


Figure 3.4: The currents through M4 and D4 and the phase current $i(\alpha)$ during one period.

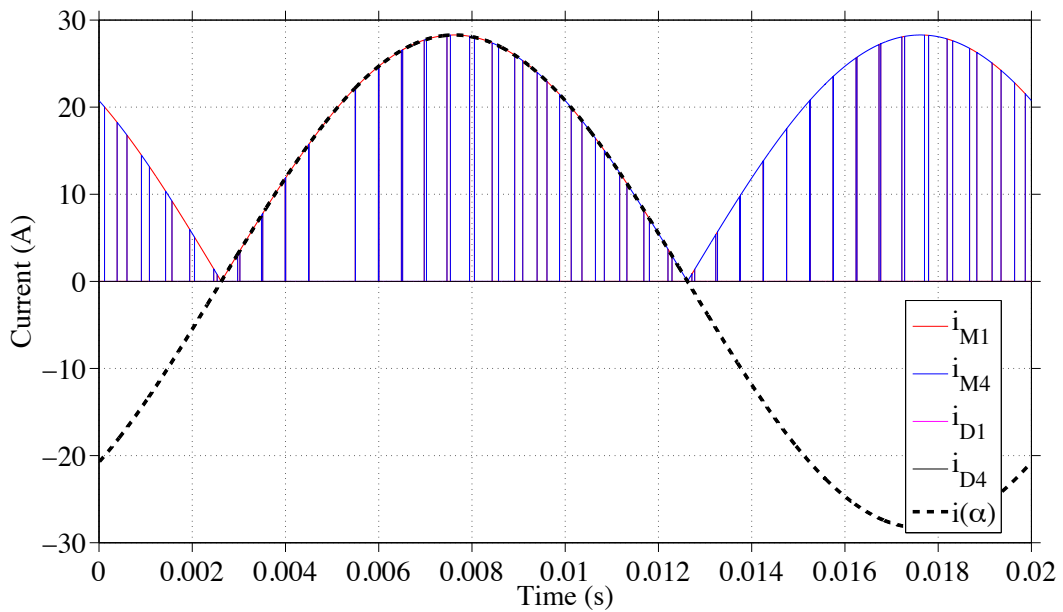


Figure 3.5: The currents through M1, D1, M4 and D4 and the phase current $i(\alpha)$ during one period when the RMS value of the phase current is 20 A.

3.2.2 Current waveforms of both MOSFET and diode conduction during high current flow in the system

Based on the same method of current simulation, when the RMS value of the phase current is increased to 150 A, which is based on the rated current of the MOSFET selected in the following chapter, the current will flow in both the MOSFETs and

the diodes. The current curves are shown in Figure 3.6 for one fundamental period. The current waveforms are in accordance with the explanation of the theory part, which shows that the diodes start conducting if the amplitude of the phase current is high enough.

From Figure 3.6, it is shown that up until a certain time instant, the diode will still not conduct even though the polarity of the current has changed. In this thesis, this start-conduction angle is called β , and will be stated and utilized in the calculation part.

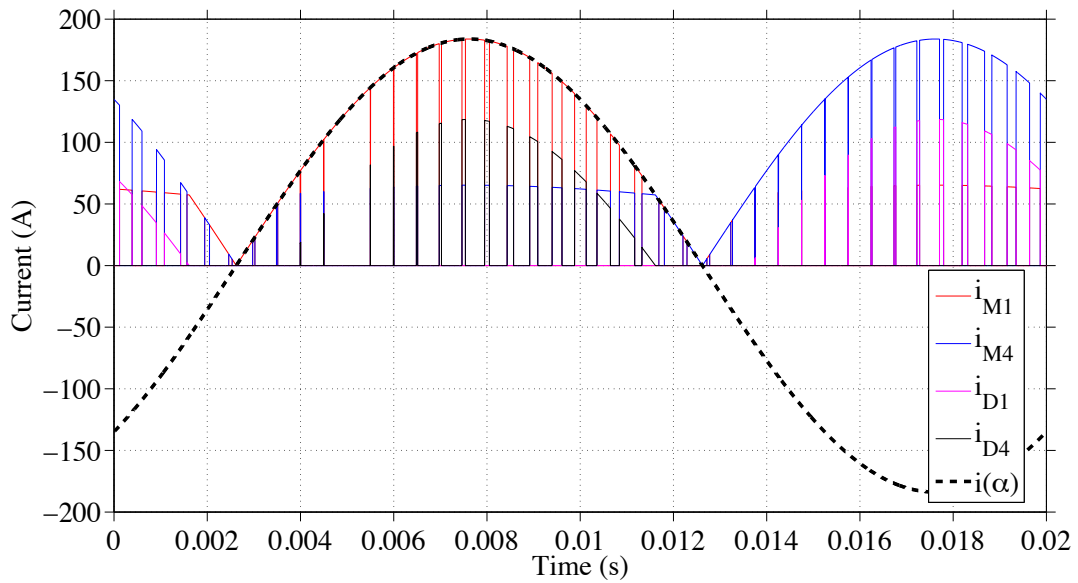


Figure 3.6: The currents through M1, D1, M4 and D4 and the phase current $i(\alpha)$ in one period when the RMS value of the phase current is 150 A.

3.3 Current analysis in the reverse conductive MOSFET

For the one-leg topology, since the current waveform is sinusoidal, thus, the upper combination of MOSFET-diode and lower combination of MOSFET-diode can be seen as symmetrical in the calculation part.

Figure 3.7 shows the details of the current waveforms through different components in one leg of the three-phase inverter when the phase current is positive. Correspondingly, Figure 3.8 is the topology which also presents the current flow during different time intervals. For instance, during time d , only M1 is conducting with the same value as the phase current. During time $(1-d)$, M4 and D4 are both conducting, and the sum of those two currents equals the phase current, $i(\alpha)$.

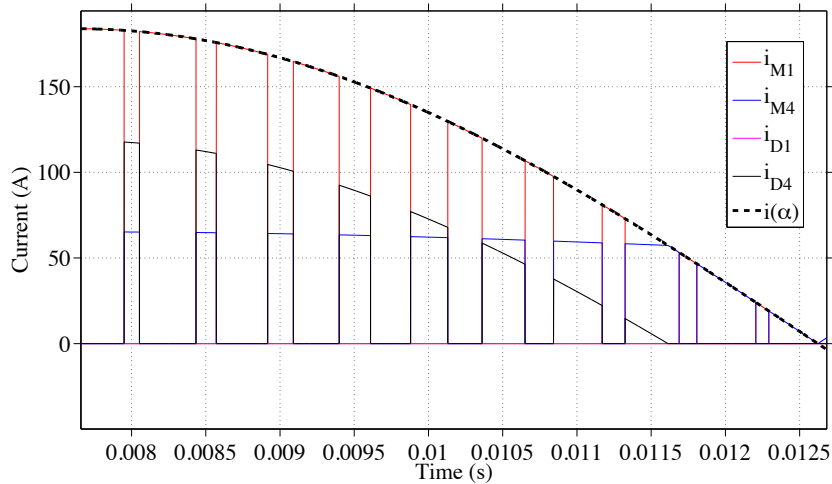


Figure 3.7: Zoomed in current waveforms: When the current is positive, the figure shows the currents through the upper MOSFET and lower MOSFET and diode during time d and $(1-d)$.

When the current is still positive, but the magnitude of the current is not high enough for D4 to conduct, then the current flow in the one-leg topology is shown in Figure 3.9.

If it comes to the negative half period of the phase current, the same procedure as for the positive phase current is used. The current flows are draw in Figure 3.10 and Figure 3.11 for high magnitudes of the phase current and for the low magnitude of the phase current.

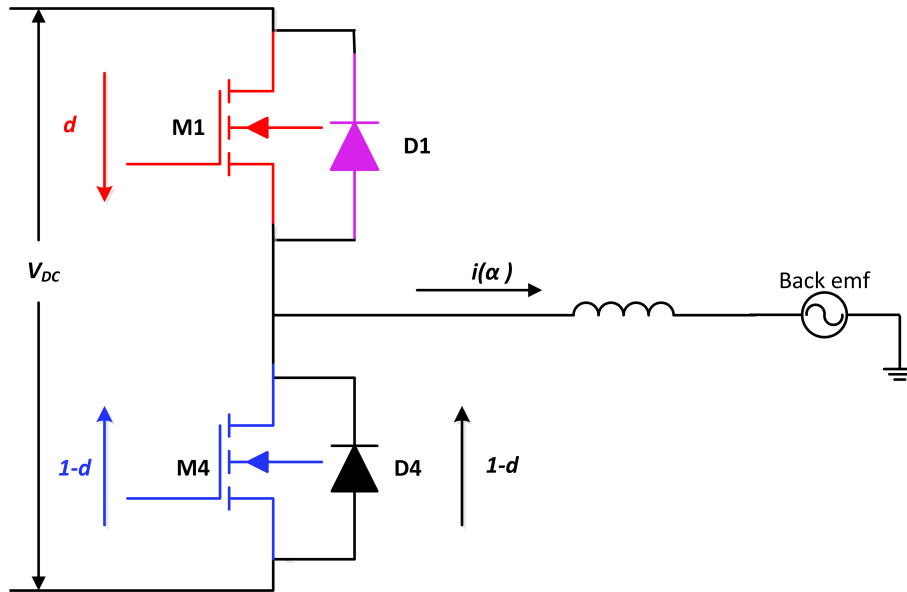


Figure 3.8: One leg topology: When the current is positive and high enough, the different directions of the currents through the upper MOSFET and lower MOSFET and diode during time d and $(1-d)$.

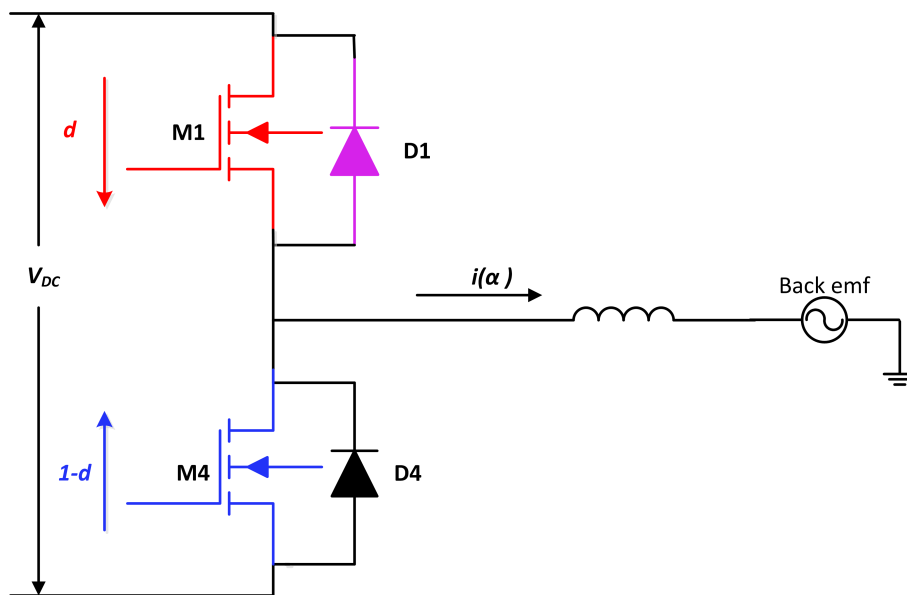


Figure 3.9: One leg topology: When the current is positive and low, the different directions of the currents through the upper MOSFET and lower MOSFET during time d and $(1-d)$.

In the following section, the current in those different time intervals will be described using mathematical expressions.

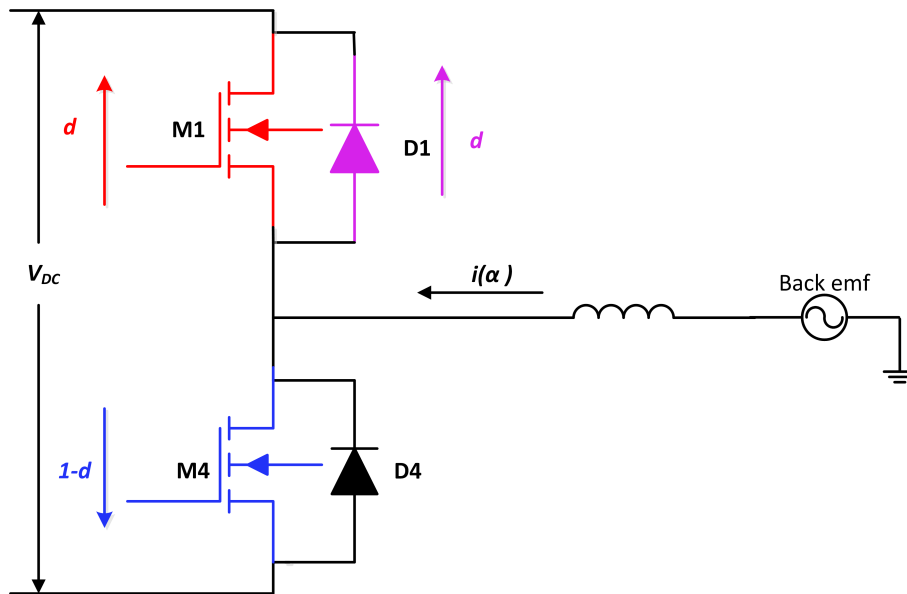


Figure 3.10: One leg topology: When the current is negative and high enough, the different directions of the currents through the upper MOSFET and lower MOSFET and diode during time d and $(1-d)$.

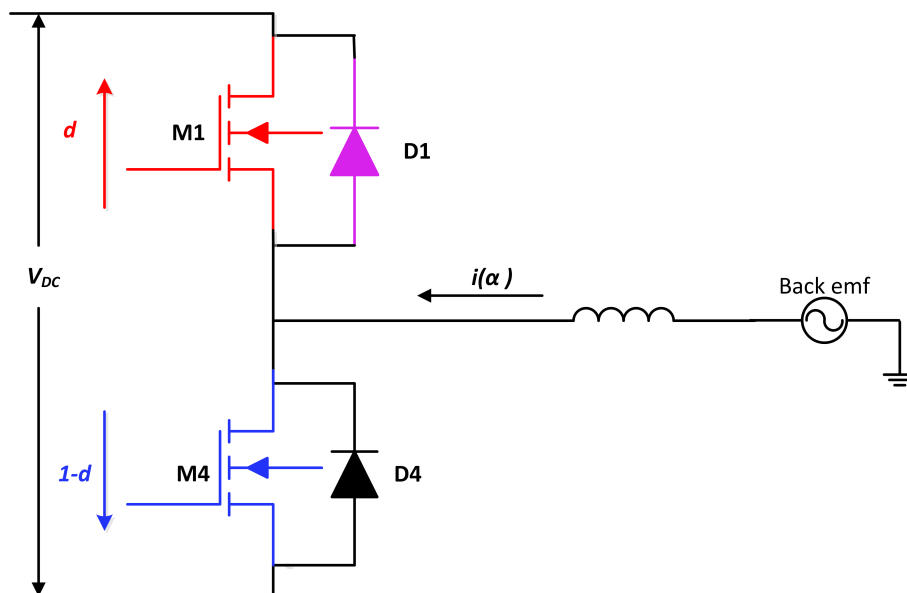


Figure 3.11: One leg topology: When the current is negative and low, the different directions of the currents through the upper MOSFET and lower MOSFET during time d and $(1-d)$.

4

Conduction Losses Calculation and Analysis

This chapter includes the mathematical explanation of the conduction losses-equations. The steps of the derivation will be presented. The calculation is based on the one-leg topology of a three-phase MOSFET inverter. The characteristics of the reverse conduction are analyzed and implemented in the final equations.

4.1 MOSFET conduction losses

The average value of the MOSFET conduction losses can be written as

$$P_{MOSFETcond} = \frac{1}{T} \int_0^T d(t)v(i(t))i(t) dt, \quad (4.1)$$

where $v(i(t))$ is the instantaneous value of the voltage over the MOSFET switch and $i(t)$ is the instantaneous value of the current through the MOSFET. The integration of the instantaneous power losses over one switching cycle thus gives an average value of the MOSFET conduction losses.

Since

$$\alpha = \frac{2\pi}{T}t, \quad (4.2)$$

Thus

$$dt = \frac{T}{2\pi}d\alpha, \quad (4.3)$$

The average value of the MOSFET conduction losses can now be determined as

$$P_{MOSFETcond} = \frac{1}{2\pi} \int_0^{2\pi} d(\alpha)v(i(\alpha))i(\alpha) d\alpha. \quad (4.4)$$

An approximation of the drain-source on-state resistance, R_{on} , is made when the calculation is derived as mentioned in Chapter 2. Thus,

$$v(i(\alpha)) = R_{on}(i(\alpha))i(\alpha), \quad (4.5)$$

Therefore, (4.4) can be rewritten as

$$P_{MOSFETcond} = \frac{1}{2\pi} \int_0^{2\pi} d(\alpha)R_{on}i^2(\alpha) d\alpha. \quad (4.6)$$

where

$$d(\alpha) = \frac{1}{2}(1 + M \sin \alpha). \quad (4.7)$$

where M is the modulation index [9]. Equation (4.6) is written in the form for later use when deriving the expression of diode losses.

4.2 Diode conduction losses

The average value of the diode conduction losses can be derived using the same method as that of the MOSFET, which is

$$P_{diodecond} = \frac{1}{T} \int_0^T d(t)v_d(i(t))i(t) dt, \quad (4.8)$$

where $v(i(t))$ is the instantaneous value of the voltage over the diode and $i(t)$ is the instantaneous value of the current through the diode. The integration of the instantaneous power losses over one fundamental cycle thus gives an average value of the losses in the diode.

Using the same procedure as (4.2) and (4.3), the average value of the diode conduction losses can now be determined as

$$P_{diodecond} = \frac{1}{2\pi} \int_0^{2\pi} d(\alpha)v_d(i(\alpha))i(\alpha) d\alpha. \quad (4.9)$$

An approximation with the resistance, R_d , and voltage drop, V_d , is made when the calculation is derived.

Thus,

$$v_d(i(\alpha)) = (R_d i(\alpha) + V_d) i(\alpha). \quad (4.10)$$

Therefore, (4.9) can be rewritten as

$$P_{diode} = \frac{1}{2\pi} \int_0^{2\pi} d(\alpha)(R_d i^2(\alpha) + V_d i(\alpha)) d\alpha, \quad (4.11)$$

Equation (4.11) is written in the form for later use when deriving the expression of diode losses.

4.3 Equations of conduction power losses during different time interval

As it is stated in Chapter 3, since the output current waveform is sinusoidal, thus, the upper package and lower package can be seen having the same power losses in

the calculation part. In this chapter, all the calculations are based on the current analysis presented in Figure 3.3 to Figure 3.7.

4.3.1 The expressions of MOSFET conduction losses in one period

Since all the figures above are taking the voltage as a reference, so in Figure 4.1 there is an angle difference between the voltage and the current, φ , where $\cos \varphi$ is the displacement power factor of the electric drive system. As it is shown in Figure 4.1, the angle from the current zero-crossing angle to the angle when the diode starts conducting, is called β . According to the symmetrical theory, the angle between the instance when the diode ends conducting and the next zero-crossing angle is also β .

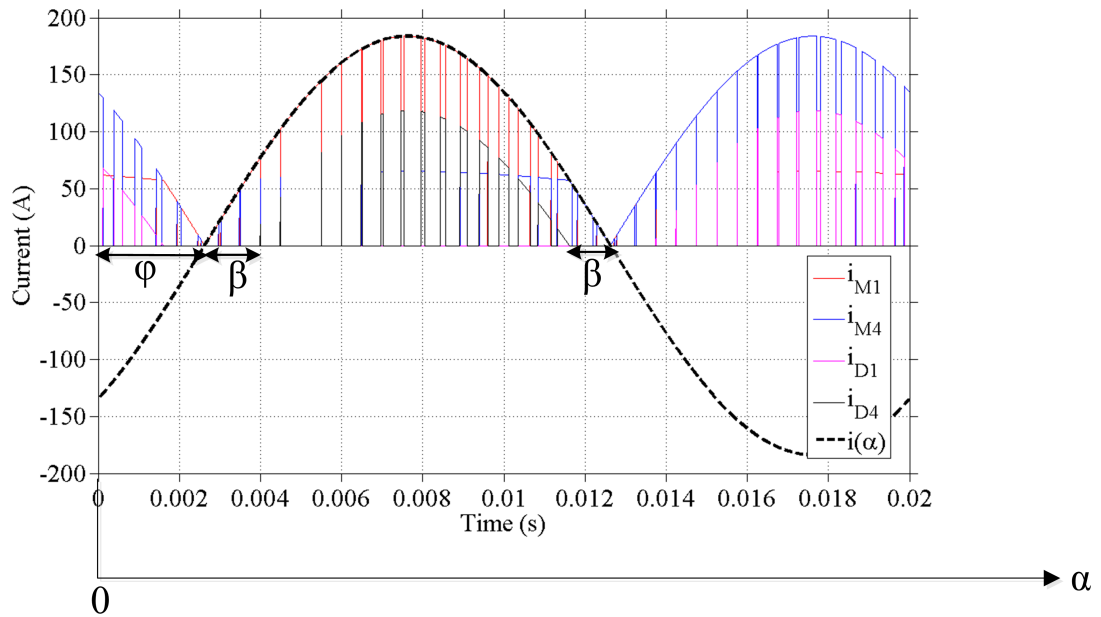


Figure 4.1: The currents waveforms of one period where the RMS value of the phase current is 150 A. φ is the angle of the displacement power factor. β is the angle between the zero-crossing angle and the angle when the diode starts conducting.

Thus, for one MOSFET, for example M1, the conduction losses can be divided to three terms, which can be written as

$$\begin{aligned}
 P_{MOSFET_{cond}} &= \frac{1}{2\pi} \int_{\varphi}^{\pi+\varphi+\beta} d(\alpha)v(i(\alpha))i(\alpha) d\alpha \\
 &+ \frac{1}{2\pi} \int_{\pi+\varphi+\beta}^{2\pi+\varphi-\beta} d(\alpha)v(i(\alpha))i(\alpha) d\alpha \\
 &+ \frac{1}{2\pi} \int_{2\pi+\varphi-\beta}^{2\pi+\varphi} d(\alpha)v(i(\alpha))i(\alpha) d\alpha.
 \end{aligned} \tag{4.12}$$

The duty cycle differs from each angle, however, the expression of the duty cycle

$$d_1 = \frac{1}{2}(1 + M \sin \alpha_1) \quad (4.13)$$

is the same if only one point is considered. Besides, the voltage expressions can be rewritten using the equations of the current. Therefore, the only difference of those three parts is the currents during different time intervals.

Since only the MOSFET is conducting in the first term and the third term of (4.12), the expressions of the current through the MOSFET have the same form as the phase current. For the second term of (4.12), the sum of the currents through the MOSFET and the diode equals the phase current. Moreover, the voltage over the MOSFET and the voltage over the diode have the same value. Therefore, the expressions of the currents through the MOSFET and the diode can be calculated as

$$i_{MOSFET} = \frac{R_d \hat{I} \sin(\alpha - \varphi) - V_d}{R_{on} + R_d} \quad (4.14)$$

and

$$i_{diode} = \frac{R_{on} \hat{I} \sin(\alpha - \varphi) + V_d}{R_{on} + R_d} \quad (4.15)$$

where \hat{I} is the peak value of the phase current.

4.3.2 The expressions of diode conduction losses in one period

Based on Figure 4.1, each diode conducts for less than half a period. For instance, D4 conducts from $\pi + \varphi + \beta$ to $2\pi + \varphi - \beta$, and the current expression has already been derived in the last section. Thus the conduction losses of the diode during one period can be written as

$$\begin{aligned} P_{diodecond} &= 0 \\ &+ \frac{1}{2\pi} \int_{\pi+\varphi+\beta}^{2\pi+\varphi-\beta} d(\alpha) v_d(i(\alpha)) i(\alpha) d\alpha \\ &+ 0 \end{aligned} \quad (4.16)$$

where the current expression of the diode is the same as (4.15).

4.3.3 Boundary condition when the diode starts conducting

Since the final equation will be implemented in MATLAB, it is better to utilize one expression which can merge two conditions of different current levels into one mathematical expression. Therefore, the boundary condition is significant.

In this work, the boundary condition is shown as below,

$$\hat{I} \sin \beta = \frac{V_d}{R_{on}}. \quad (4.17)$$

The boundary condition of β can be defined using (4.17). With the settings of β , the losses-equations will be valid for all the calculation, no matter if the current is high enough or not for the diodes conducting.

4.4 Total Conduction losses equations during one period

From Section 4.3.1 and Section 4.3.2, the total conduction losses of the MOSFET can be expressed using the equations of the power losses, (4.12) and (4.16), and the expressions of the currents, (4.14) and (4.15). Thus the expression of the MOSFET losses can be rewritten as

$$\begin{aligned} P_{MOSFETcond} &= \frac{1}{2\pi} \int_{\varphi}^{\pi+\varphi+\beta} \frac{1}{2} (1 + M \sin \alpha) R_{on} \hat{I}^2 \sin^2(\alpha - \varphi) d\alpha \\ &+ \frac{1}{2\pi} \int_{\pi+\varphi+\beta}^{2\pi+\varphi-\beta} \frac{1}{2} (1 + M \sin \alpha) R_{on} \left(\frac{R_d \hat{I} \sin(\alpha - \varphi) - V_d}{(R_{on} + R_d)^2} \right)^2 d\alpha \quad (4.18) \\ &+ \frac{1}{2\pi} \int_{2\pi+\varphi-\beta}^{2\pi+\varphi} \frac{1}{2} (1 + M \sin \alpha) R_{on} \hat{I}^2 \sin^2(\alpha - \varphi) d\alpha. \end{aligned}$$

Using the same method, the diode losses during one period can be expressed as

$$\begin{aligned} P_{diodecond} &= \frac{1}{2\pi} \int_{\pi+\varphi+\beta}^{2\pi+\varphi-\beta} \frac{1}{2} (1 + M \sin \alpha) \\ &\left[V_d \left(- \frac{R_{on} \hat{I} \sin(\alpha - \varphi) + V_d}{R_{on} + R_d} \right) + R_d \left(\frac{R_{on} \hat{I} \sin(\alpha - \varphi) + V_d}{R_{on} + R_d} \right)^2 \right] d\alpha. \end{aligned} \quad (4.19)$$

The expressions shown above are straightforward to understand according to (4.12) and (4.16). Regarding the implementation in MATLAB, the speed of running the calculation needs to be taken into consideration. One way to improve the computation speed is to derive a simpler algorithmic calculation instead of the integration for MATLAB. To derive those algebraic expressions, the expressions need to be integrated. However, due to the asymmetry of the conduction behavior of the MOSFET and the diode in the positive half period and the negative half period, the simplified algebraic equations are more complicated than the ones of an IGBT inverter in [4]. The reason of the complexity is the angle β , which means that the MOSFETs conduct more than half of a period during the whole period. Moreover, during the reverse conduction of the MOSFET, the phase current is divided into two expressions for the MOSFET and the diode. The expressions of the currents shown in

(4.14) and (4.15) give more complicated results than using the expression of the phase current in the IGBT losses-calculation.

The derived losses-equations of the MOSFET can be written as

$$\begin{aligned}
 P_{MOSFETcond} = & \frac{1}{8\pi} \hat{I}^2 R_{on} \left[\pi + \beta + M \cos(\varphi + \beta) + M \cos \varphi - \frac{1}{2} \sin 2\beta \right. \\
 & \left. + \frac{M}{2} \cos(\varphi - \beta) + \frac{M}{2} \cos \varphi - \frac{M}{6} \cos(\varphi + 3\beta) - \frac{M}{6} \cos \varphi \right] \\
 & + \frac{1}{8\pi} \hat{I}^2 R_{on} \left[\beta - M \cos \varphi + M \cos(\varphi - \beta) - \frac{1}{2} \sin 2\beta \frac{M}{2} \cos \varphi \right. \\
 & \left. + \frac{M}{2} \cos(\varphi + \beta) + \frac{M}{6} \cos \varphi - \frac{M}{6} \cos(\varphi - 3\beta) \right] \\
 & + \frac{1}{4\pi} \frac{R_{on}}{(R_{on} + R_d)^2} \left\{ R_d^2 \hat{I}^2 (2\pi - 4\beta + 2 \sin 2\beta) + V_d^2 (\pi - 2\beta) \right. \\
 & + 4R_d \hat{I} \cos \beta \\
 & + \frac{1}{12} M R_d^2 \hat{I}^2 \left[-9 \cos(\beta - \varphi) - 9 \cos(\beta + \varphi) \right. \\
 & \left. + \cos(3\beta - \varphi) + \cos(3\beta + \varphi) \right] - M V_d^2 \left[\cos(\varphi - \beta) + \cos(\varphi + \beta) \right] \\
 & \left. - \frac{1}{2} M R_d \hat{I} \left[(2\pi - 4\beta) \cos \varphi + \sin(2\beta - \varphi) + \sin(2\beta + \varphi) \right] \right\}. \tag{4.20}
 \end{aligned}$$

The derived losses-equations of the diode can be written as

$$\begin{aligned}
 P_{diodecond} = & \frac{1}{4\pi} \frac{1}{(R_d + R_{on})^2} \left[\frac{1}{2} M (R_{on} - R_d) (-V_d) R_{on} \hat{I} ((\pi - 2\beta) \cos \varphi \right. \\
 & \left. + \sin(2\beta - \varphi) + \sin(2\beta + \varphi) \right] + M V_d^2 R_{on} \left[\cos(\varphi - \beta) \right. \\
 & \left. + \cos(\varphi + \beta) \right] + \frac{1}{12} M R_d R_{on}^2 \hat{I}^2 \left[-9 \cos(\varphi + \beta) - 9 \cos(\varphi - \beta) \right. \\
 & \left. + \cos(\varphi - 3\beta) + \cos(\varphi + 3\beta) \right] \\
 & + 2(R_{on} - R_d) V_d R_{on} \hat{I} \cos \beta \\
 & - V_d^2 R_{on} (\pi - 2\beta) + \frac{1}{4} R_d R_{on}^2 \hat{I}^2 (2\pi - \beta + 2 \sin 2\beta). \tag{4.21}
 \end{aligned}$$

Equation (4.20) and (4.21) give the same results as the expressions in (4.18) and (4.19). Furthermore, the results are needed to be verified through another method of power losses calculation, which will be explained in the next chapter.

5

Verification Using Numerical Analysis

5.1 Prerequisites of the numerical analysis

In this chapter, numerical calculations are performed in MATLAB to verify the theoretical losses-equations. The MOSFET module, CAS300M12BM2 from CREE, is selected in the numerical calculation for the following reasons. CAS300M12BM2 has a rated current of 300 A, which is high enough for a three-phase MOSFET inverter of an electric drive system. The drain-source voltage of CAS300M12BM2 can reach 1.2 kV. Due to the better switching performance of the MOSFET, the switching frequency, f_{sw} , is selected to be 20 kHz in the calculation. The DC voltage is set to be 400 V in this case, which can be selected as the DC voltage of the inverter in an electric drive system. However, with the development of the Silicon carbide (SiC) devices, the components chosen in this project can be used also for higher voltage levels, such as hybrid buses or trucks.

Based on the schematic circuit of CAS300M12BM2, the corresponding data of the anti-parallel diode can be obtained from the data sheet of the MOSFET module [11]. Table 5.1 presents the equivalent values of the voltage drop and the resistances which are used in the following calculations [12].

Table 5.1: Set up of the simulation.

Name	Value
I_{rms}	150A
V_{DC}	400V
f_{sw}	20kHz
f_1	50Hz
R_{on}	0.0098 Ω
V_d	0.75V
R_d	0.005 Ω

5.2 Numerical losses calculation

5.2.1 Calculation procedure

To calculate the conduction losses numerically, a reasonable time step should be set. The fundamental period is 0.02 s. In this verification, the time step is selected to be 0.1 μ s, from which each discrete sample of voltage and current are used to calculate the losses.

Figure 5.1 shows the phase current and the MOSFET conduction losses using the numerical calculation. Each point represents the instantaneous losses at the sampled time. When the phase current is at a high value, the losses is at a higher level. Correspondingly, when the amplitude of the phase current is low, the losses is at a lower level. The conduction losses of the MOSFET exist during the whole period.

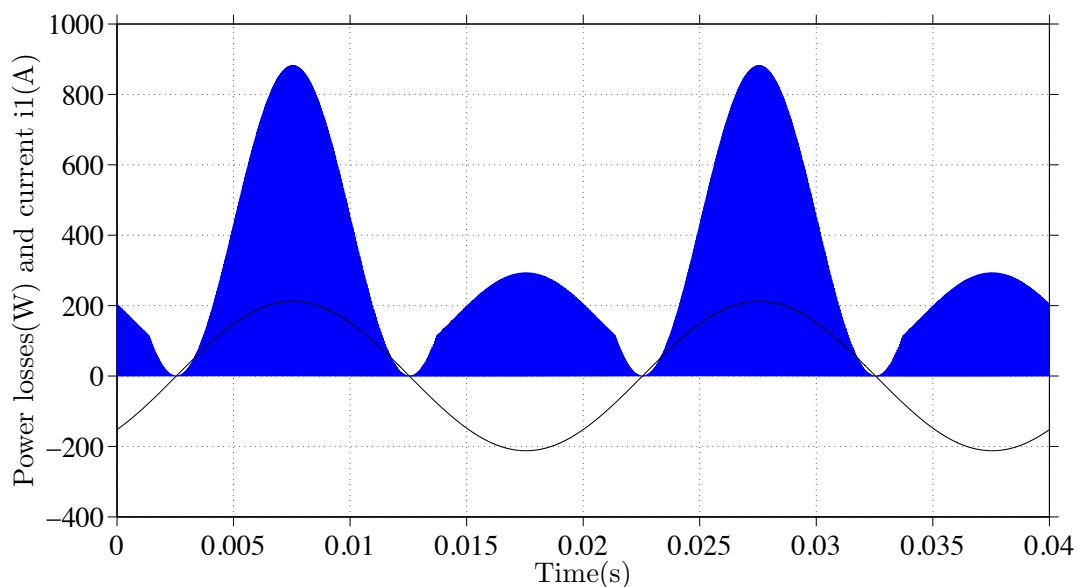


Figure 5.1: The phase current and MOSFET losses during two periods, when the current is high enough for the diode to conduct.

The corresponding diode conduction losses are shown in Figure 5.2. From Figure 5.1 and Figure 5.2, it can be seen that when the diode generates losses, the losses in the MOSFET increase moderately.

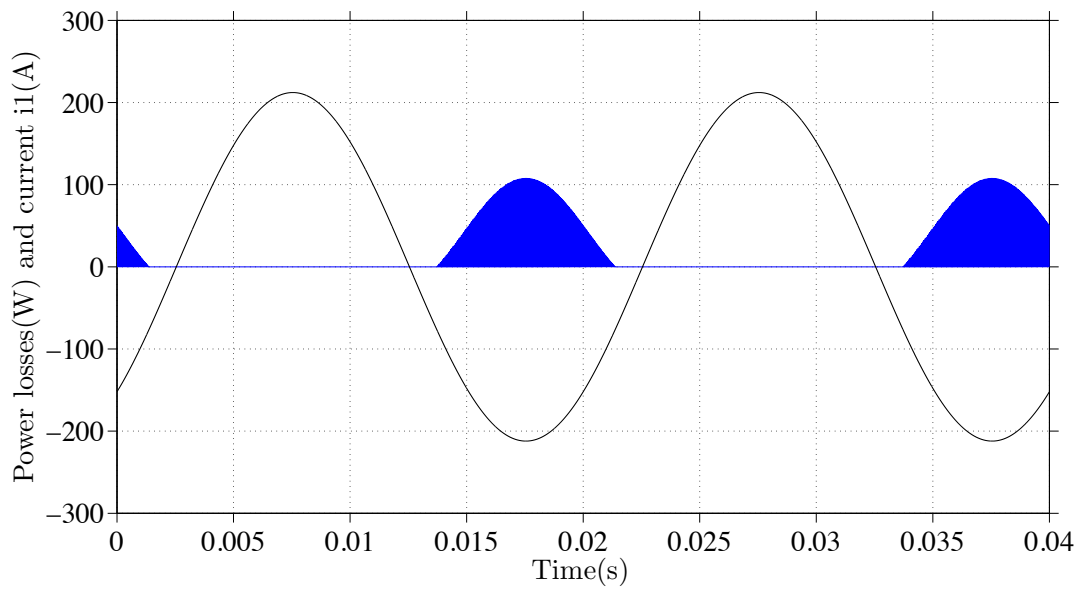


Figure 5.2: The phase current and diode losses during two periods.

5.2.2 Results of the numerical reference system and verification with theoretical calculation

The results from the analytical and numerical calculation are presented and compared in Table 5.2 to Table 5.5. The RMS value of the phase current is 150 A in this case. The examples of the verification are selected to show the results from the two different methods. In addition, the differences of each MOSFET and diode losses between the analytical calculation and numerical calculation are given in the tables.

Table 5.2: Calculation results when $M = 0.7$ and $\varphi = 0.82$.

Component	Analytical Losses(W)	Numerical Losses(W)	Difference (%)
MOSFET	89.82	89.83	0.01
Diode	7.80	7.80	0

Table 5.3: Calculation results when $M = 0.6$ and $\varphi = 0.8$.

Component	Analytical Losses(W)	Numerical Losses(W)	Difference (%)
MOSFET	91.53	91.52	0.01
Diode	7.16	7.16	0

Table 5.4: Calculation results when $M = 1$ and $\varphi = 0$.

Component	Analytical Losses(W)	Numerical Losses(W)	Difference (%)
MOSFET	106.54	106.55	0.01
Diode	1.49	1.49	0

Table 5.5: Calculation results when $M = 1$ and $\varphi = \pi$.

Component	Analytical Losses(W)	Numerical Losses(W)	Difference (%)
MOSFET	49.08	49.09	0.02
Diode	23.17	23.16	-0.04

To make the verification having an overall consideration, another value of the phase current is necessary to be selected below the diode conduction threshold. In this case, the power losses are calculated when the RMS value of the phase current is 20 A. The results are shown in Table 5.6.

Table 5.6: Calculation results when $M = 1$ and $\varphi = 0$ with $I_{rms} = 20A$.

Component	Analytical Losses(W)	Numerical Losses(W)	Difference (%)
MOSFET	1.96	1.96	0
Diode	0	0	0

All the differences shown in Table 5.2 to Table 5.6 are not more than 0.04%. It indicates that the theoretical expressions and the numerical reference system agree with each other. The two methods can be used to calculate the conduction losses in the MOSFET three-phase inverter.

6

Theoretical Analysis and Comparison between MOSFET with reverse conduction and without reverse conduction

6.1 Theoretical analysis of the mathematical equations with MOSFET reverse conduction

The relations between φ , M , and the conduction losses are shown in Figure 6.1 and Figure 6.2. In this simulation, I_{rms} is 150 A, which makes both of the diode and the MOSFET conducting. It can be seen that the conduction losses of the MOSFET vary following a cosine function of φ , while the conduction losses of the diode follows a (-cosine) function of φ . Even though those two equations have opposite tendency, the total losses in one MOSFET-diode module shown in Figure 6.1 give the similar tendency as the conduction losses of the MOSFET. In addition, the conduction losses of the MOSFET increase linearly as M increases. However, the conduction losses of the diode decrease when M increases. Since the conduction losses in the diodes are lower than the ones in the MOSFET within one module, the total losses in one module shown in Figure 6.1 and Figure 6.2 have the similar tendency as that of the MOSFET.

6. Theoretical Analysis and Comparison between MOSFET with reverse conduction and without reverse conduction

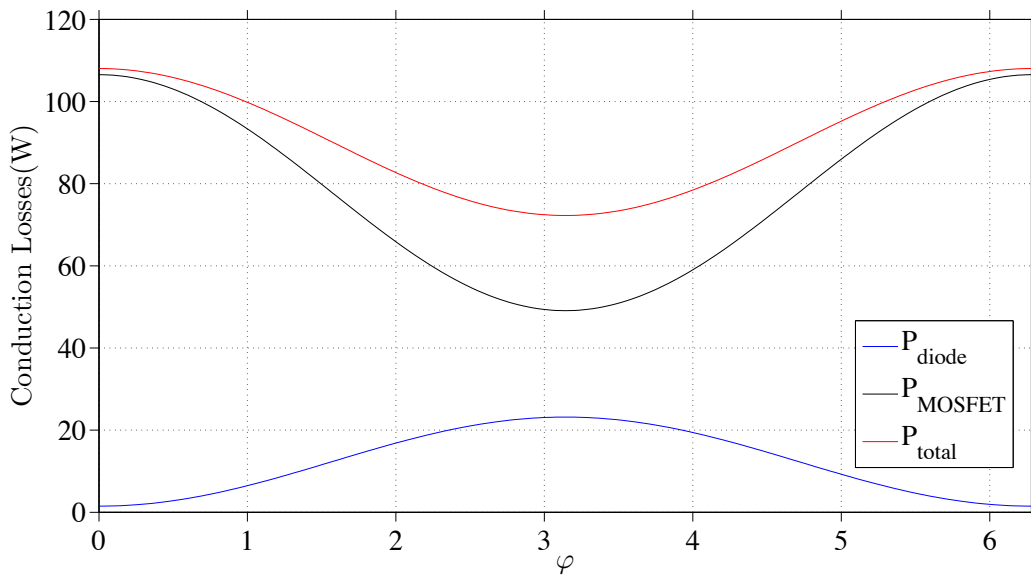


Figure 6.1: The relation between MOSFET conduction losses and ϕ when $M = 1$ with reverse conduction characteristics.

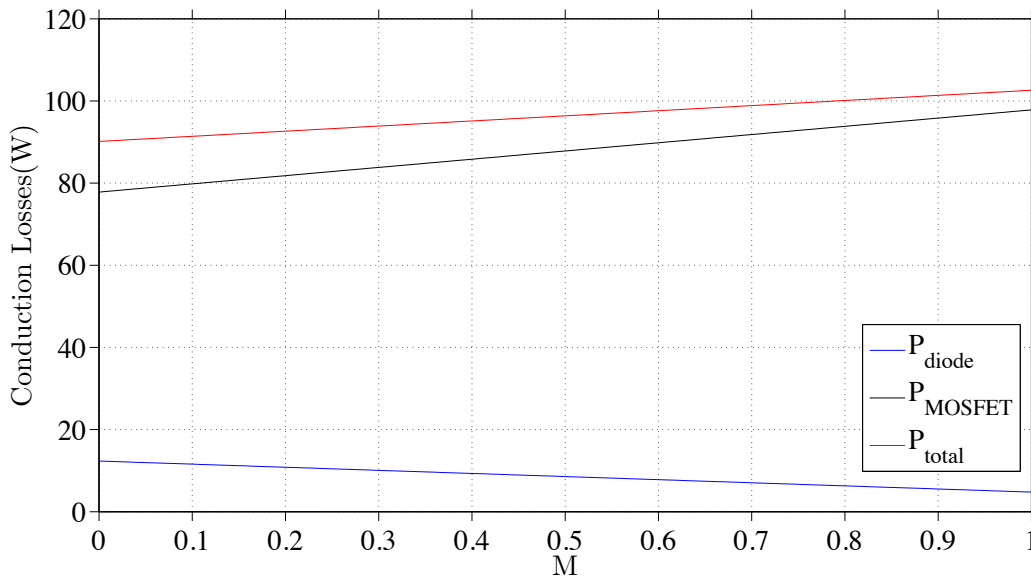


Figure 6.2: The relation between MOSFET conduction losses and ϕ when $M = 1$ with reverse conduction characteristics.

6.2 Comparison and analysis between MOSFET with reverse conduction and without reverse conduction

According to the analysis in previous chapters, the complexity of the equations of the MOSFET inverter is due to that the reverse conduction can be utilized. Thus, it is necessary to find out the difference between the losses resulting with reverse conduction and without reverse conduction. Table 6.1 and Table 6.2 present both MOSFET and diode losses for different values of M , when I_{rms} is 150 A and φ is 0.8. The total differences are calculated and shown in Table 6.3.

Table 6.1: MOSFET losses with and without reverse conducting when I_{rms} is 150 A.

M	Losses with reverse conducting(W)	Losses without reverse conducting(W)
0	77.81	55.12
0.2	81.81	61.65
0.4	85.81	68.16
0.6	89.81	74.68
0.8	93.82	81.20
1	97.82	87.73

Table 6.2: Diode losses with or without MOSFET reverse conducting when I_{rms} is 150 A.

M	Losses with reverse conducting(W)	Losses without reverse conducting(W)
0	12.33	53.44
0.2	10.82	47.34
0.4	9.31	41.25
0.6	7.80	35.15
0.8	6.29	29.06
1	4.78	22.96

Since the value of the total losses in one MOSFET-diode module is relevant for the loss evaluation in the inverter, the differences are calculated and compared in Table 6.3. As it can be seen above, the MOSFET with reverse conduction characteristics makes the total conduction losses in one module less than the assumption without reverse conduction. It is due to that the conduction losses depend mainly on the currents through the components instead of other factors, such as the voltages over the components or the equivalent resistance of the components. If a lower current is applied to this kind of inverter, for instance I_{rms} is 20 A, the differences are shown in Table 6.4 to Table 6.6. In that case, there are much less conduction losses in one module than the case without reverse conduction. The current dependency can also

6. Theoretical Analysis and Comparison between MOSFET with reverse conduction and without reverse conduction

Table 6.3: Total losses with or without MOSFET reverse conducting when I_{rms} is 150 A.

M	Total losses with reverse conducting(W)	Total losses without reverse conducting(W)	Difference(%)
0	90.14	108.57	+20.45
0.2	92.63	108.99	+17.66
0.4	95.12	109.41	+15.02
0.6	97.62	109.84	+12.52
0.8	100.11	110.26	+10.14
1	102.60	110.68	+7.88

be verified in the next chapter when using different forms of reference voltages in the inverter.

Table 6.4: MOSFET losses with and without reverse conducting when I_{rms} is 20 A.

M	Losses with reverse conducting(W)	Losses without reverse conducting(W)
0	1.96	0.98
0.2	1.96	1.09
0.4	1.96	1.21
0.6	1.96	1.32
0.8	1.96	1.44
1	1.96	1.56

Table 6.5: Diode losses with or without MOSFET reverse conducting when I_{rms} is 20 A.

M	Losses with reverse conducting(W)	Losses without reverse conducting(W)
0	0	3.87
0.2	0	3.44
0.4	0	3.02
0.6	0	2.59
0.8	0	2.16
1	0	1.73

6. Theoretical Analysis and Comparison between MOSFET with reverse conduction and without reverse conduction

Table 6.6: Total losses with or without MOSFET reverse conducting when I_{rms} is 20 A.

M	Total losses with reverse conducting(W)	Total losses without reverse conducting(W)	Difference(%)
0	1.96	4.86	+147.96
0.2	1.96	4.54	+131.63
0.4	1.96	4.23	+115.82
0.6	1.96	3.91	+99.49
0.8	1.96	3.60	+83.67
1	1.96	3.29	+67.86

6. Theoretical Analysis and Comparison between MOSFET with reverse conduction and without reverse conduction

7

Conduction Losses Calculation using two different PWM Methods

In this chapter, the results from two different PWM methods will be calculated using the numerical system and compared to the results obtained in Chapter 6.

7.1 Numerical results with the third harmonic injection

7.1.1 Reference voltage design principle

The third harmonic injection PWM (THIPWM) is a common way to utilize the DC voltage source in the system [13] [14]. Since the THIPWM can make more use of the DC voltage source than the PWM method using the pure sinusoidal reference voltages, this section presents the losses using THIPWM [16].

Figure 7.1 shows the reference voltages under THIPWM. For instance, one phase of the reference voltages is composed by

$$u_{THIPWMA} = \hat{U} \sin(\omega t) + 0.17\hat{U} \sin(3\omega t). \quad (7.1)$$

Equation (7.1) is used in the losses calculation in this section.

7.1.2 Results and comparison

The different losses using THIPWM are calculated using various φ , when M is fixed, as well as various M when φ is a fixed value. The results are shown in Table 7.1, Table 7.2, Table 7.3 and Table 7.4.

The differences can be seen by comparing the total losses in one MOSFET-diode module with or without THIPWM, for example when $\varphi = 0.8$ and $M = 0.6$, the total losses using a pure sinusoidal reference voltages are 97.62 W in Table 6.3, and the losses with THIPWM are 98.07 (90.50 + 7.57) W. The new total losses will increase by 0.46%. Based on (4.12) and (4.16), the losses mostly depend on the current flowing through the components. However, when the reference voltages change the

7. Conduction Losses Calculation using two different PWM Methods

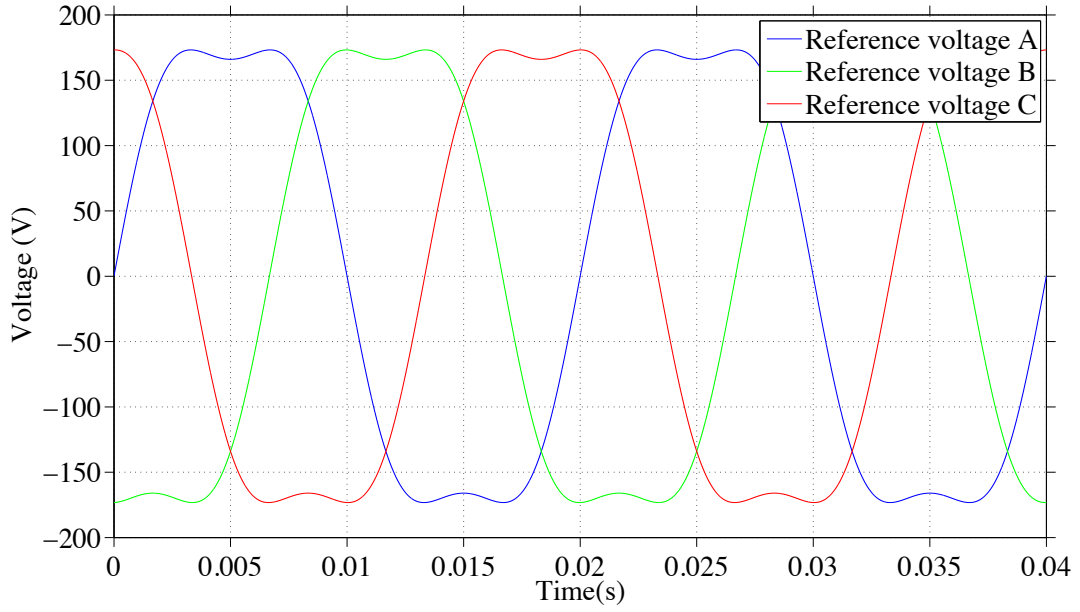


Figure 7.1: Three phase reference voltages with the third harmonic injection .

Table 7.1: Results without third harmonic injection when $M = 0.6$.

φ	MOSFET losses(W)	Diode losses(W)
0	95.03	5.83
0.8	89.81	7.80
1	87.11	8.82
1.8	73.89	13.81
π	60.58	18.84

Table 7.2: Results with third harmonics injection when $M = 0.6$.

φ	MOSFET losses(W)	Difference(%)	Diode losses(W)	Difference(%)
0	94.11	-0.97	6.15	5.48
0.8	90.50	0.76	7.57	-2.94
1	88.04	1.07	8.51	-3.51
1.8	73.31	-0.70	14.01	1.45
π	61.51	1.54	18.51	-1.75

expressions, there are different forms of the duty cycle in the formula. The expressions under different reference voltages are suggested to be valuable for the future work of research.

Table 7.3: Results without third hamonics injection when $\varphi = 0$.

M	MOSFET losses(W)	Diode losses(W)
0	77.50	12.28
0.2	83.53	10.17
0.4	89.28	8.00
0.6	95.03	5.83
0.8	100.78	3.66
1	106.52	1.49

Table 7.4: Results with third hamonics injection when $\varphi = 0$.

M	MOSFET losses(W)	Difference(%)	Diode losses(W)	Difference(%)
0	77.50	0	12.28	0
0.2	83.23	-0.36	10.27	0.98
0.4	88.68	-0.67	8.21	2.63
0.6	94.10	0.97	6.14	5.31
0.8	99.57	-1.20	4.07	11.20
1	104.99	-1.44	2.01	34.89

7.2 Results with the common mode reduction

7.2.1 Voltage design principle

There is another method to utilize the DC voltage source in the system in the best way, which is the common mode reduction. In this study, the common mode is chosen to be the symmetrical triangular wave. The PWM method is based on sinusoidal waveforms with reduced common mode. The following algorithm is used in the losses-calculation in this section.

The common mode, C_m , is defined as

$$C_m = (umin + umax)/2. \quad (7.2)$$

In (7.2), the value of $umin$ is the minimum value of the three-phase sinusoidal reference voltages, and the value of $umax$ is the maximum value of those three voltages. Thus, the three-phase reference voltages can be written as

$$u_{asym} = \hat{U} \sin(\omega t) - C_m \quad (7.3)$$

$$u_{bsym} = \hat{U} \sin(\omega t - 120^\circ) - C_m \quad (7.4)$$

$$u_{csym} = \hat{U} \sin(\omega t - 240^\circ) - C_m. \quad (7.5)$$

The reference voltages under symmetrical triangular wave injection are shown in Figure 7.2. The losses are calculated and compared in the following section.

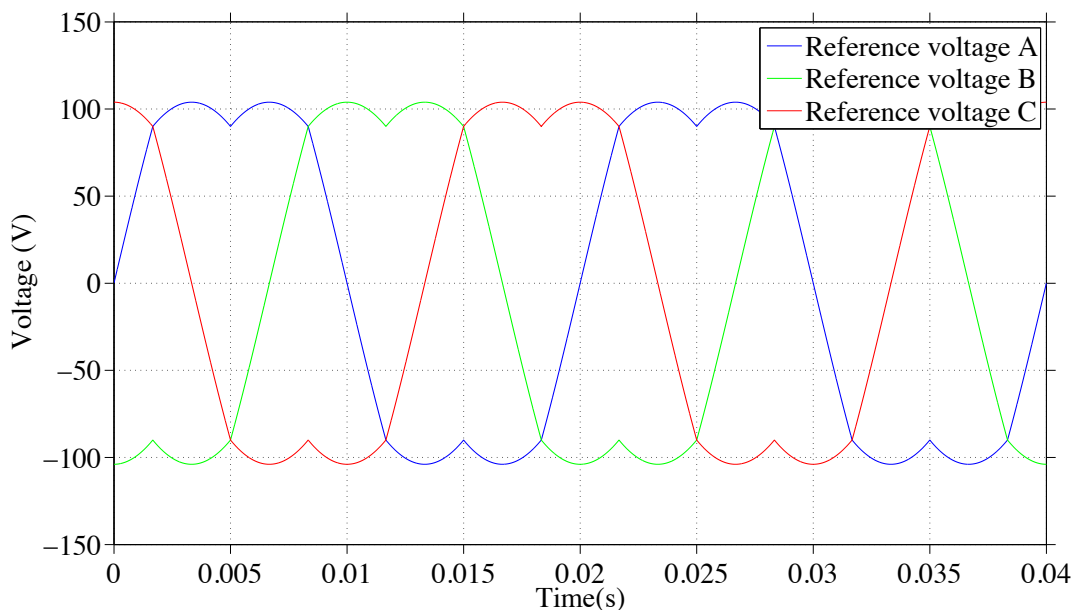


Figure 7.2: Three phase reference voltages with the symmetrical triangular wave injection.

7.2.2 Results and comparison

The results of losses using the symmetrical triangular wave injection are calculated using the same method as used when determining the losses in the THIPWM case. The results are shown in Table 7.5, Table 7.6, Table 7.7 and Table 7.8.

Table 7.5: Results without the symmetrical triangular wave injection when $M = 0.6$.

φ	MOSFET losses(W)	Diode losses(W)
0	95.03	5.83
0.8	89.81	7.80
1	87.11	8.82
1.8	73.89	13.81
π	60.58	18.84

The differences can be seen by comparing the total losses in one MOSFET-diode module with or without the common mode reduction, for example when $\varphi = 0.8$ and $M = 0.6$, the total losses using a pure sinusoidal reference voltages are 97.62 W in Table 6.3, and the losses with the common mode reduction are 98.16 W (90.50 + 7.57 W) . The new total losses will increase by 0.55%. Based on (4.12) and (4.16), the losses mostly depend on the current flowing through the components. However, when the reference voltages change, there are different forms of the duty cycle in the formula. Those questions is suggested to be a valuable future research.

Table 7.6: Results with the symmetrical triangular wave injection when $M = 0.6$.

φ	MOSFET losses(W)	Difference(%)	Diode losses(W)	Difference(%)
0	93.90	-1.19	6.21	6.52
0.8	90.64	0.92	7.52	-3.59
1	88.23	1.28	8.43	-4.42
1.8	73.18	-0.96	14.05	1.74
π	61.72	1.88	18.44	-2.12

Table 7.7: Results without symmetrical triangular wave injection when $\varphi = 0$.

M	MOSFET losses(W)	Diode losses(W)
0	77.50	12.28
0.2	83.53	10.17
0.4	89.28	8.00
0.6	95.03	5.83
0.8	100.78	3.66
1	106.52	1.49

Table 7.8: Results with the symmetrical triangular wave injection when $\varphi = 0$.

M	MOSFET losses(W)	Difference(%)	Diode losses(W)	Difference(%)
0	77.50	0	12.28	0
0.2	83.17	-0.43	10.29	1.18
0.4	88.55	-0.82	8.24	1.03
0.6	93.90	1.19	6.21	6.51
0.8	99.28	-1.49	4.17	13.93
1	104.66	-1.75	2.13	42.95

7. Conduction Losses Calculation using two different PWM Methods

8

Conclusion

It can be concluded that the theoretical equations of the conduction losses show good agreement with the results from the numerical reference system. The derived losses-equations can be implemented in MATLAB for the future losses calculation. Moreover, the conduction losses in one MOSFET-diode combination have a similar tendency of the MOSFET, regardless of M or φ . The reverse conduction of the MOSFET gives lower conduction losses in one module compared to not using reverse conduction. Without the reverse conduction, the losses of one power module are higher than the case with reverse conduction at both the high and low current levels. CAS300M12BM2 is selected to be the power module in the numerical calculation. The differences are shown in tables and the losses can be more than 20 % higher than the case with reverse condition at the rated current of the selected module, 150 A. When the phase current is low and there is no diode conducting during the operation, the losses regardless of reverse conduction can be more than 100 % higher. Furthermore, the conduction losses mainly depend on the values of the currents through the components.

8. Conclusion

9

Future Work

In this work, the equations of conduction losses in a three-phase MOSFET inverter are derived. The equations are based on the reverse conduction of the MOSFET. However, the goal of the future is to derive the equations which can reflect the real system. The blanking time is significant, and it should not be neglected. Thus, the equations, with blanking time accounted for, are needed. Moreover, for the numerical reference system, further developed equations under different PWM methods will be valuable to solve. With those considerations, the conduction losses equations of the three-phase inverter model can be improved.

9. Future Work

Bibliography

- [1] Evan Hirsh, Arjun Kakkar, Akshay Singh, Reid Wilk *2015 Auto Industry Trends*. <http://www.strategyand.pwc.com/perspectives/2015-auto-trends>, Strategyand, Jan 2015.
- [2] *Tracking progress towards Kyoto and 2020 targets in Europe*. <http://www.eea.europa.eu/publications/progress-towards-kyoto>, EEA (European Environment Agency), 12 Oct 2010.
- [3] C. C. Chan. *The State of the Art of Electric, Hybrid, and Fuel Cell Vehicles*. Proceedings of the IEEE, Vol. 95, No. 4, April 2007.
- [4] SEMIKRON. *Basics Inverter Loss Calculation*. SEMIKRON innovation service, 2009.
- [5] Tiefu Zhao, Jun Wang, Alex Q. Huang. *Comparisons of SiC MOSFET and Si IGBT Based Motor Drive Systems*. Cree Inc., Durham, NC 27703, USA.
- [6] Ned Mohan, Tore M. Undeland, William P. Robbins. *Power Electronics Converters, Applications, and Design*. John Wiley and Sons, INC, 2003.
- [7] K. Vinoth Kumar, Prawin Angel Michael, Joseph P. John and Dr. S. Suresh Kumar. *SIMULATION AND COMPARISON OF SPWM AND SVPWM CONTROL FOR THREE PHASE INVERTER*. I2006-2010 Asian Research Publishing Network (ARPN), VOL. 5, NO. 7, JULY 2010.
- [8] Steven Pekarek, Timothy Skvarenina. *Graphic Modeller Component Models for Electric Power Education*. Proceedings of the IEEE, 1998.
- [9] Johann W. Kolar, Hans Ertl, and Franz C. Zach. *Influence of the Modulation Method on the Conduction and Switching Losses of a PWM Converter System*. IEEE Transaction on Industry Applications, VOL. 21, NO. 6, November, December, 1991
- [10] B. Wrzecionko, D. Bortis, J. W. Kolar. *A 120 °C Ambient Temperature Forced Air-Cooled Normally-off SiC JFET Automotive Inverter System*. IEEE Transactions on Power Electronics, Vol. 29, No. 5, pp. 2345-2358, May 2014.
- [11] S. Matsumoto. *Advancement of hybrid vehicle technology*. Eur. Conf. Power Electron. Appl., Dresden, Germany, Sep. 1114, 2005.

- [12] Jih-Sheng Lai, Wensong Yu, Hao Qian, Pengwei Sun, Parish Ralston, and Kathleen Meehan. *High Temperature Device Characterization for Hybrid Electric Vehicle Traction Inverters*. 978-1-422-2812-0/09 I2009 IEEE
- [13] M.A.A. Younis, N. A. Rahim, and S. Mekhilef. *Harmonic Reduction In Three-Phase Parallel Connected Inverter*. World Academy of Science, Engineering and Technology 50 2009.
- [14] I. J. Pitel, S. N. Talukdar, and P. Wood. *Characterization of Programmed-Waveform Pulse-Width Modulation*. IEEE Transactions on Industry Applications, Vol. IA-16, Sept./Oct. 1980, pp. 707715.
- [15] Ken Berringer, Jeff Marvin, Philippe Perruchoud *Semiconductor Power Losses in AC Inverters*. Industry Applications Conference, 1995. Thirtieth IAS Annual Meeting, IAS '95, Conference Record of the 1995 IEEE, Oct 1995.
- [16] N. A. Rahim and S. Mekhilef *Simulation of Grid Connected THIPWM-Three-Phase Inverter Using SIMULINK*. IEEE Symposium on Industrial Electronics and Applications (ISIEA2011), September 25-28, 2011.
- [17] Ion Boldea, S. A. Nasar *Electric Drives*. CRC Press, LLC, 1999.

10

Appendix 1

Data sheet of CAS300M12BM2.

CAS300M12BM2

1.2kV, 5.0 mΩ All-Silicon Carbide Half-Bridge Module

C2M MOSFET and Z-Rec™ Diode

V_{DS}	1.2 kV
$E_{sw, Total @ 300A}$	12.0 mJ
$R_{DS(on)}$	5.0 mΩ

Features

- Ultra Low Loss
- High-Frequency Operation
- Zero Reverse Recovery Current from Diode
- Zero Turn-off Tail Current from MOSFET
- Normally-off, Fail-safe Device Operation
- Ease of Paralleling
- Copper Baseplate and Aluminum Nitride Insulator

System Benefits

- Enables Compact and Lightweight Systems
- High Efficiency Operation
- Mitigates Over-voltage Protection
- Reduced Thermal Requirements
- Reduced System Cost

Applications

- Induction Heating
- Motor Drives
- Solar and Wind Inverters
- UPS and SMPS
- Traction

Package 62mm x 106mm x 30mm



Part Number	Package	Marking
CAS300M12BM2	Half-Bridge Module	CAS300M12BM2

Maximum Ratings ($T_c = 25^\circ\text{C}$ unless otherwise specified)

Symbol	Parameter	Value	Unit	Test Conditions	Notes
V_{DSmax}	Drain - Source Voltage	1.2	kV		
V_{GSmax}	Gate - Source Voltage	-10/+25	V	Absolute Maximum values	
V_{GSop}	Gate - Source Voltage	-5/20	V	Recommended Operational Values	
I_D	Continuous Drain Current	404	A	$V_{GS} = 20\text{ V}, T_c = 25^\circ\text{C}$	Fig. 24
		285		$V_{GS} = 20\text{ V}, T_c = 90^\circ\text{C}$	
$I_{D(pulse)}$	Pulsed Drain Current	1500	A	Pulse width $t_p = 200\ \mu\text{s}$ Repetition rate limited by $T_{jmax}, T_c = 25^\circ\text{C}$	
T_{Jmax}	Junction Temperature	150	$^\circ\text{C}$		
T_c, T_{STG}	Case and Storage Temperature Range	-40 to +125	$^\circ\text{C}$		
V_{isol}	Case Isolation Voltage	4.0	kV	AC, 50 Hz, 1 min	
L_{Stray}	Stray Inductance	14	nH	Measured between terminals 2 and 3	
P_D	Power Dissipation	1660	W	$T_c = 25^\circ\text{C}, T_J = 150^\circ\text{C}$	Fig. 23



Electrical Characteristics ($T_c = 25^\circ\text{C}$ unless otherwise specified)

Symbol	Parameter	Min.	Typ.	Max.	Unit	Test Conditions	Note
$V_{(BR)DSS}$	Drain - Source Breakdown Voltage	1.2			kV	$V_{GS} = 0\text{ V}, I_D = 1\text{ mA}$	
$V_{GS(th)}$	Gate Threshold Voltage	1.8	2.3		V	$V_{DS} = 10\text{ V}, I_D = 15\text{ mA}$	Fig 7
I_{DSS}	Zero Gate Voltage Drain Current		500	2000	μA	$V_{DS} = 1.2\text{ kV}, V_{GS} = 0\text{V}$	
			1000			$V_{DS} = 1.2\text{ kV}, V_{GS} = 0\text{V}, T_J = 150^\circ\text{C}$	
I_{GSS}	Gate-Source Leakage Current		1	100	nA	$V_{GS} = 20\text{ V}, V_{DS} = 0\text{V}$	
$R_{DS(on)}$	On State Resistance		5.0	5.7	m Ω	$V_{GS} = 20\text{ V}, I_{DS} = 300\text{ A}$	Fig. 4, 5, 6
			8.6	9.8		$V_{GS} = 20\text{ V}, I_{DS} = 300\text{ A}, T_J = 150^\circ\text{C}$	
g_{fs}	Transconductance		94.8		S	$V_{DS} = 20\text{ V}, I_{DS} = 300\text{ A}$	Fig. 8
			93.3			$V_{DS} = 20\text{ V}, I_D = 300\text{ A}, T_J = 150^\circ\text{C}$	
C_{iss}	Input Capacitance		11.7		nF	$V_{DS} = 600\text{ V}, f = 200\text{ kHz}, V_{AC} = 25\text{ mV}$	Fig. 16, 17
C_{oss}	Output Capacitance		2.55				
C_{rss}	Reverse Transfer Capacitance		0.07				
E_{on}	Turn-On Switching Energy		6.05		mJ	$V_{DD} = 600\text{ V}, V_{GS} = -5\text{V}/+20\text{V}$ $I_D = 300\text{ A}, R_{G(ext)} = 2.5\ \Omega$ Note: IEC 60747-8-4 Definitions	Fig. 19, 20
E_{off}	Turn-Off Switching Energy		5.95		mJ		
$R_{G(int)}$	Internal Gate Resistance		3.0		Ω	$f = 200\text{ kHz}, V_{AC} = 25\text{ mV}$	
Q_{GS}	Gate-Source Charge		166		nC	$V_{DD} = 800\text{ V}, V_{GS} = -5\text{V}/+20\text{V}, I_D = 300\text{ A},$ Per JEDEC24 pg 27	Fig. 15
Q_{GD}	Gate-Drain Charge		475				
Q_G	Total Gate Charge		1025				
$t_{d(on)}$	Turn-on delay time		76		ns	$V_{DD} = 600\text{V}, V_{GS} = -5/+20\text{V}, I_D = 300\text{ A}, R_{G(ext)} = 2.5\ \Omega,$ Timing relative to V_{DS} Note: IEC 60747-8-4, pg 83 Inductive load	Fig. 25
t_r	Rise Time		68		ns		
$t_{d(off)}$	Turn-off delay time		168		ns		
t_f	Fall Time		43		ns		

Free-Wheeling SiC Schottky Diode Characteristics

Symbol	Parameter	Min.	Typ.	Max.	Unit	Test Conditions	Note
V_{SD}	Diode Forward Voltage		1.7	2.0	V	$I_F = 300\text{ A}, V_{GS} = 0$	Fig. 9, 10, 11
			2.2	2.5		$I_F = 300\text{ A}, T_J = 150^\circ\text{C}, V_{GS} = 0$	
Q_C	Total Capacitive Charge		3.2		μC		

Note: The reverse recovery is purely capacitive

Thermal Characteristics

Symbol	Parameter	Min.	Typ.	Max.	Unit	Test Conditions	Note
R_{thJCM}	Thermal Resistance Junction-to-Case for MOSFET		0.070	0.075	$^\circ\text{C}/\text{W}$	$T_c = 90^\circ\text{C}, P_D = 150\text{ W}$	Fig. 27, 28
R_{thJCD}	Thermal Resistance Junction-to-Case for Diode		0.073	0.076		$T_c = 90^\circ\text{C}, P_D = 130\text{ W}$	

Additional Module Data

Symbol	Parameter	Max.	Unit	Test Condition
W	Weight	300	g	
M	Mounting Torque	5	Nm	To heatsink and terminals
	Clearance Distance	12	mm	Terminal to terminal
	Creepage Distance	30	mm	Terminal to terminal
		40	mm	Terminal to baseplate

Typical Performance

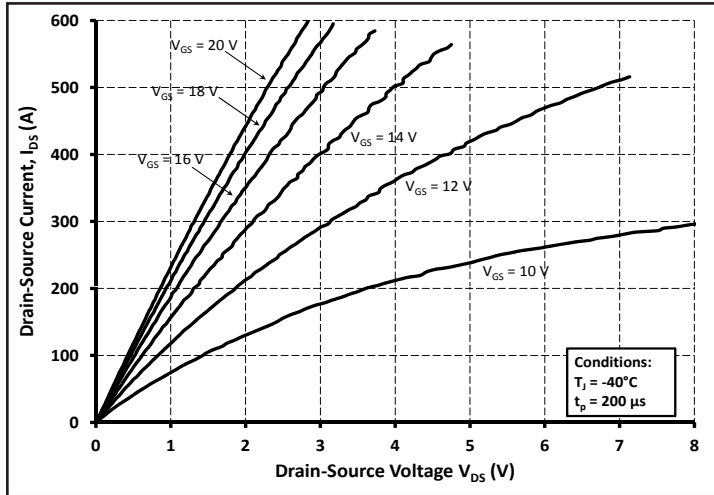


Figure 1. Typical Output Characteristics $T_j = -40\text{ }^\circ\text{C}$

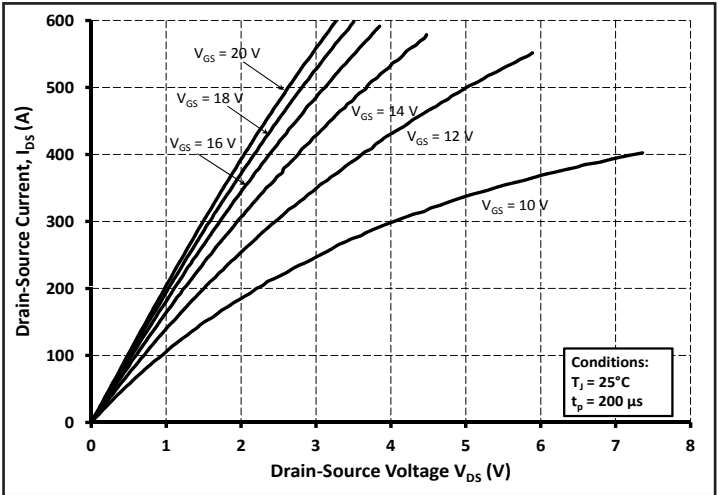


Figure 2. Typical Output Characteristics $T_j = 25\text{ }^\circ\text{C}$

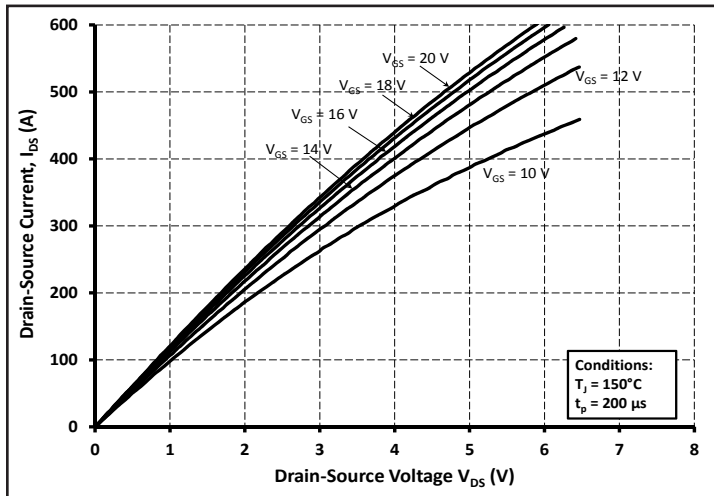


Figure 3. Typical Output Characteristics $T_j = 150\text{ }^\circ\text{C}$

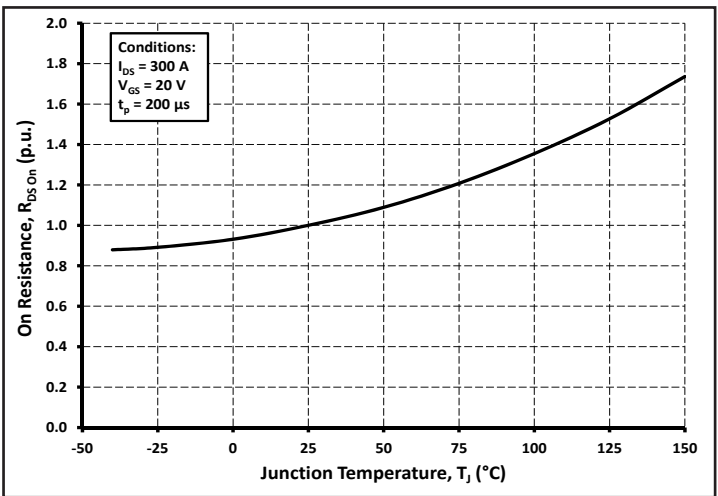


Figure 4. Normalized On-Resistance vs. Temperature

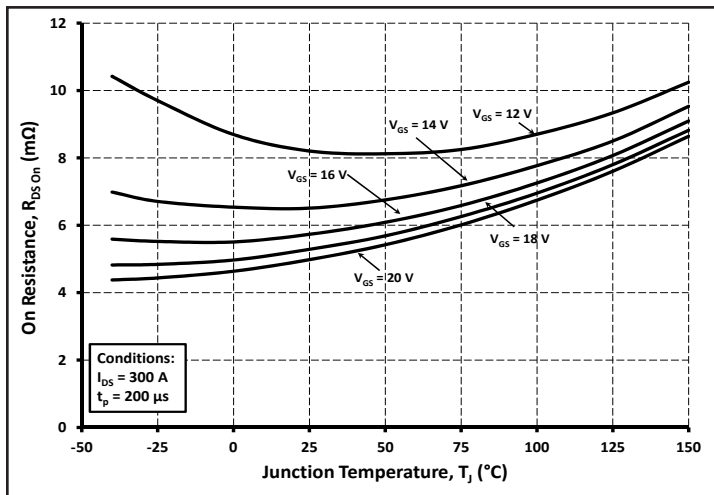


Figure 5. Typical On-Resistance vs. Temperature for Various Gate-Source Voltage

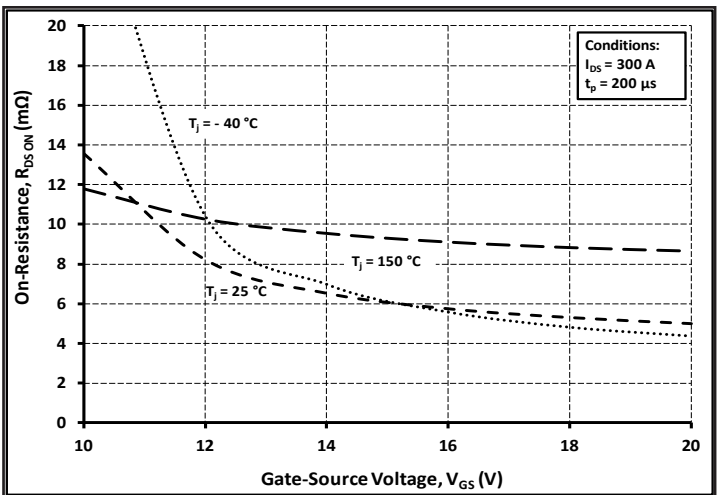


Figure 6. Typical On-Resistance vs. Gate Voltage

Typical Performance

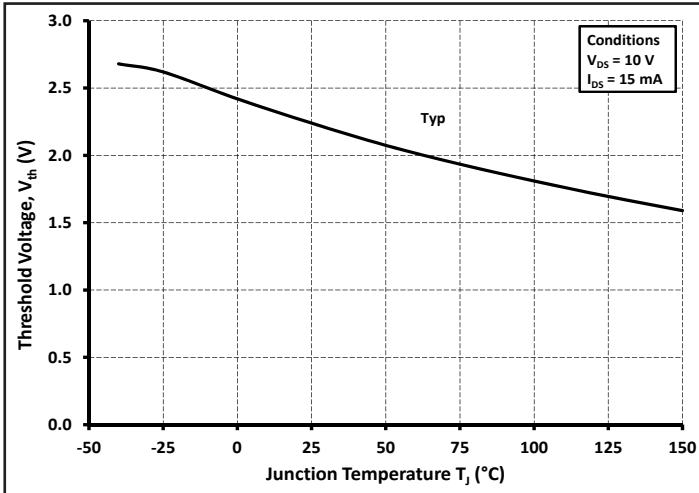


Figure 7. Threshold Voltage vs. Temperature

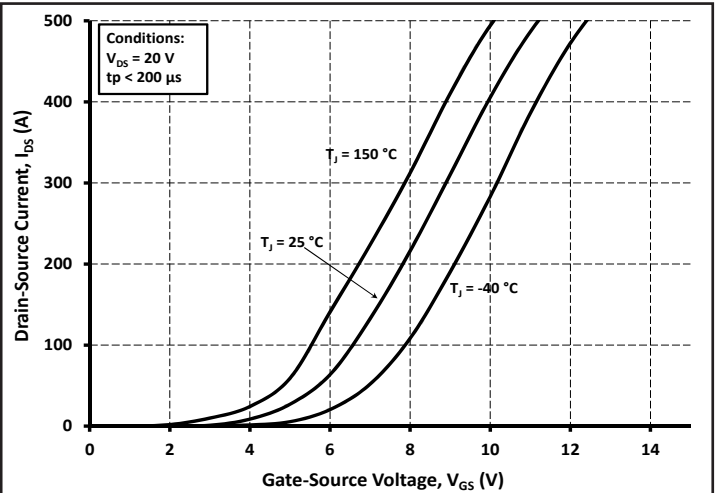


Figure 8. Transfer Characteristic for Various Junction Temperatures

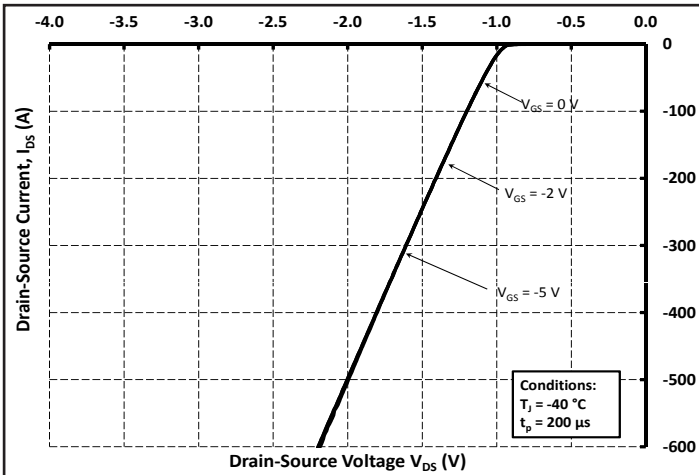


Figure 9. Diode Characteristic at $-40\text{ }^\circ\text{C}$

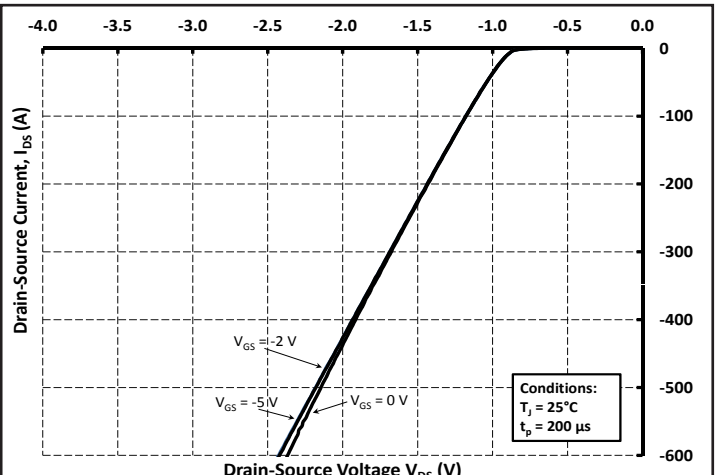


Figure 10. Diode Characteristic at $25\text{ }^\circ\text{C}$

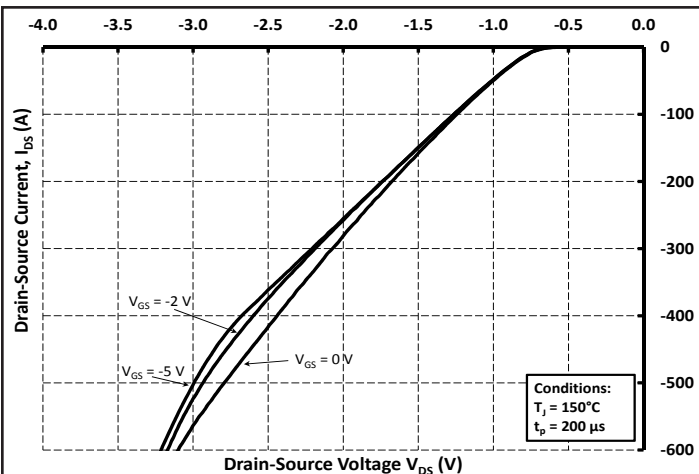


Figure 11. Diode Characteristic at $150\text{ }^\circ\text{C}$

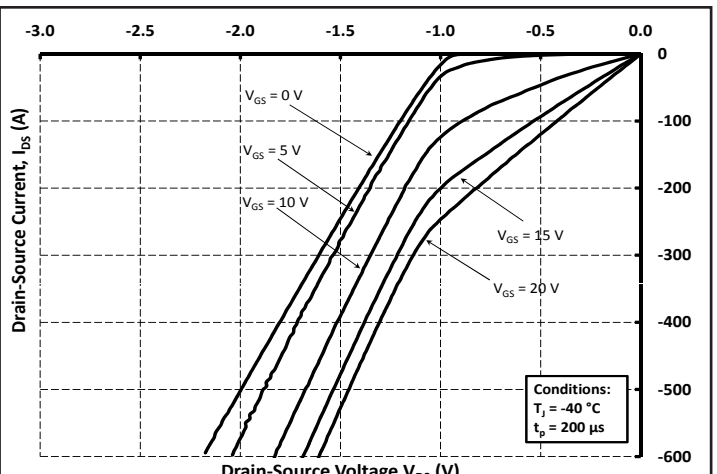


Figure 12. 3rd Quadrant Characteristic at $-40\text{ }^\circ\text{C}$

Typical Performance

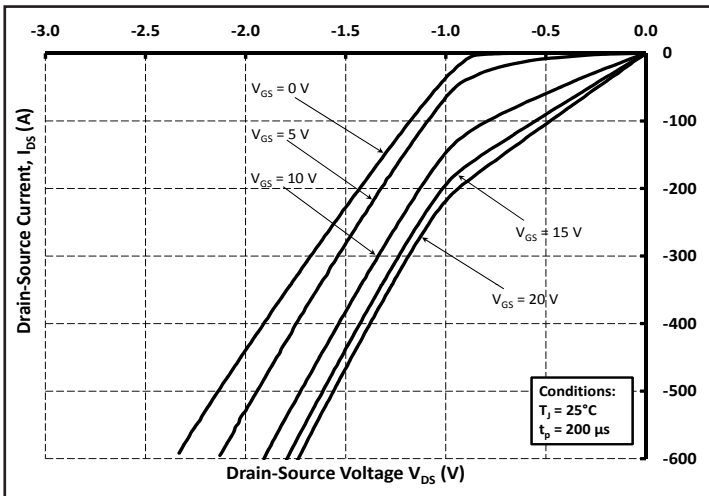


Figure 13. 3rd Quadrant Characteristic at 25 °C

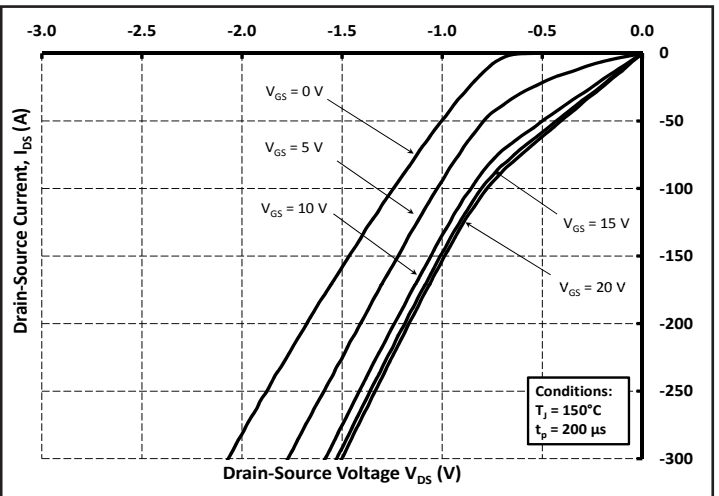


Figure 14. 3rd Quadrant Characteristic at 150 °C

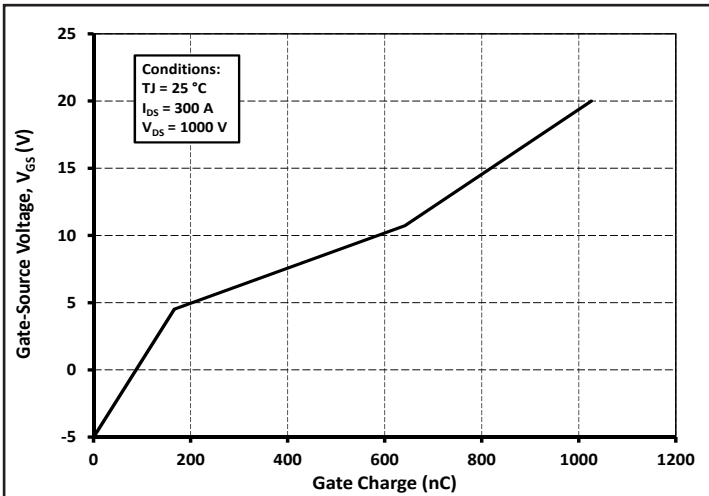


Figure 15. Typical Gate Charge Characteristics

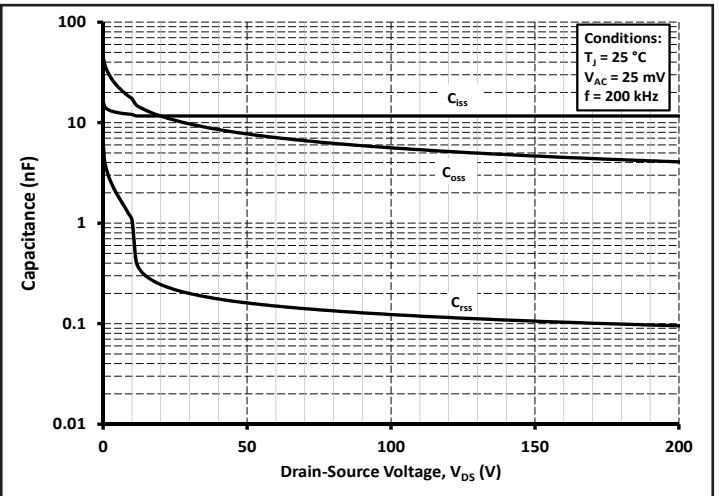


Figure 16. Typical Capacitances vs. Drain-Source Voltage (0 - 200 V)

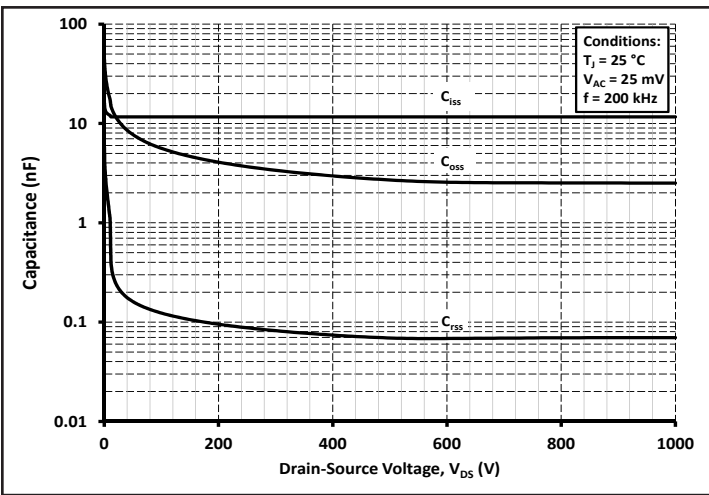


Figure 17. Typical Capacitances vs. Drain-Source Voltage (0 - 1 kV)

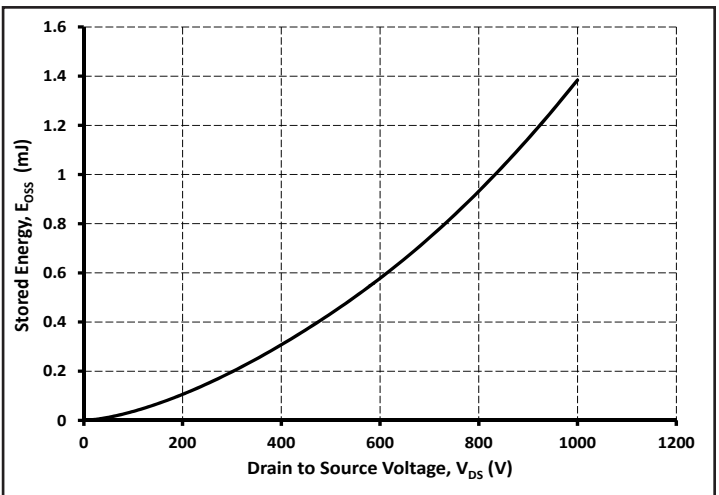


Figure 18. Typical Output Capacitor Stored Energy

Typical Performance

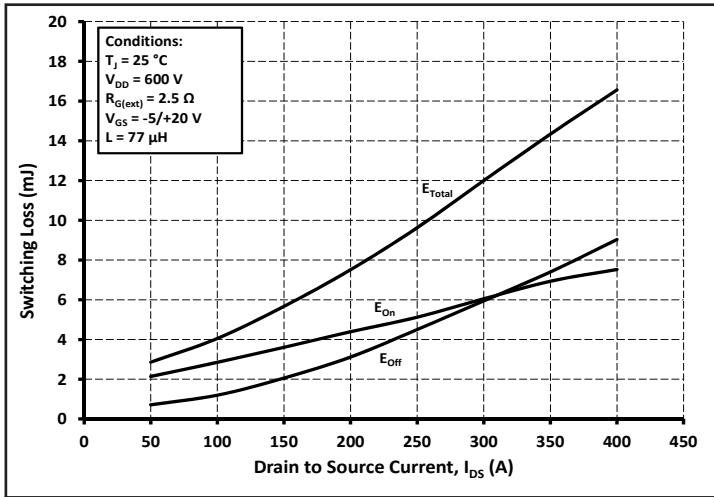


Figure 19. Inductive Switching Energy vs. Drain Current For $V_{DS} = 600V$, $R_G = 2.5 \Omega$

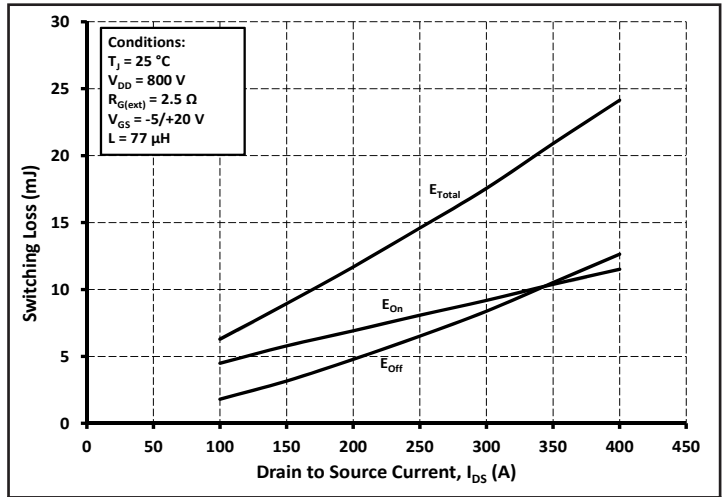


Figure 20. Inductive Switching Energy vs. Drain Current For $V_{DS} = 800V$, $R_G = 2.5 \Omega$

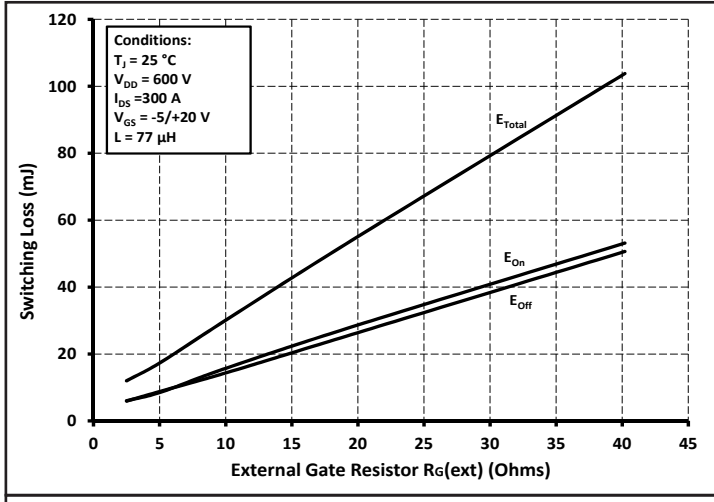


Figure 21. Inductive Switching Energy vs. $R_{G(ext)}$

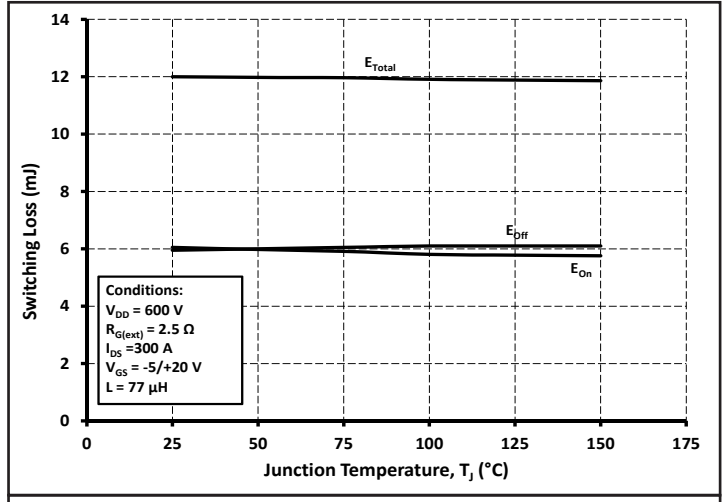


Figure 22. Inductive Switching Energy vs. Temperature

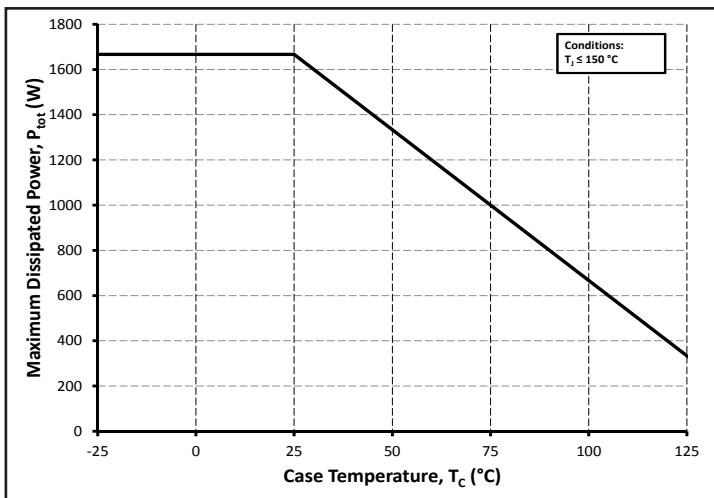


Figure 23. Maximum Power Dissipation (MOSFET) Derating vs Case Temperature

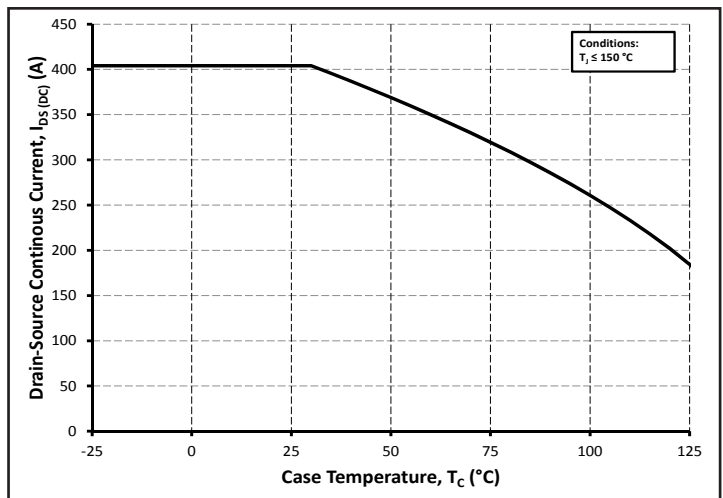


Figure 24. Continuous Drain Current Derating vs Case Temperature

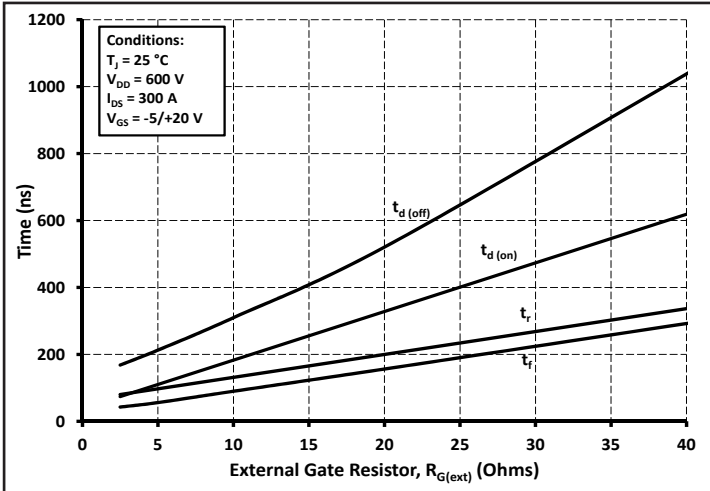


Figure 25. Timing vs. $R_{G(ext)}$

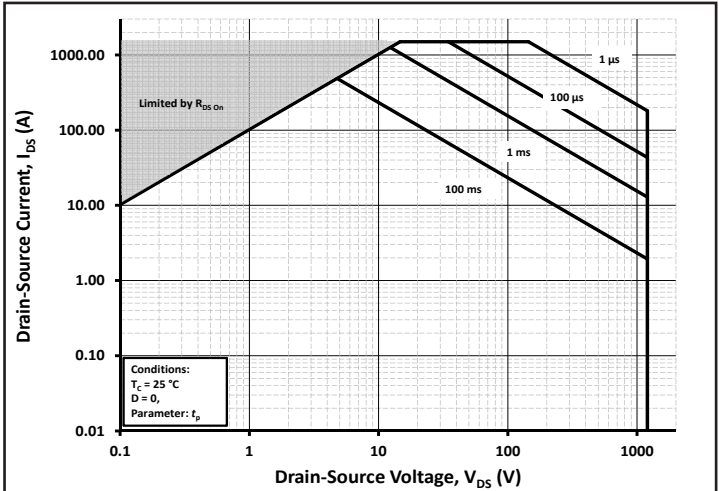


Figure 26. Continuous Drain Current Derating vs Case Temperature

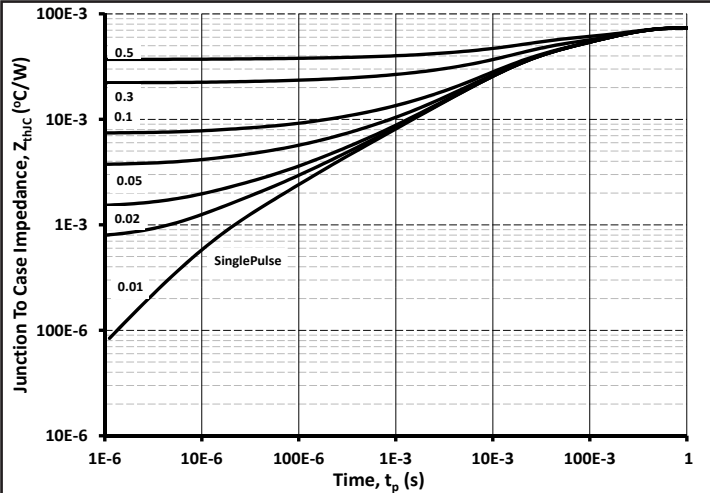


Figure 27. MOSFET Junction to Case Thermal Impedance

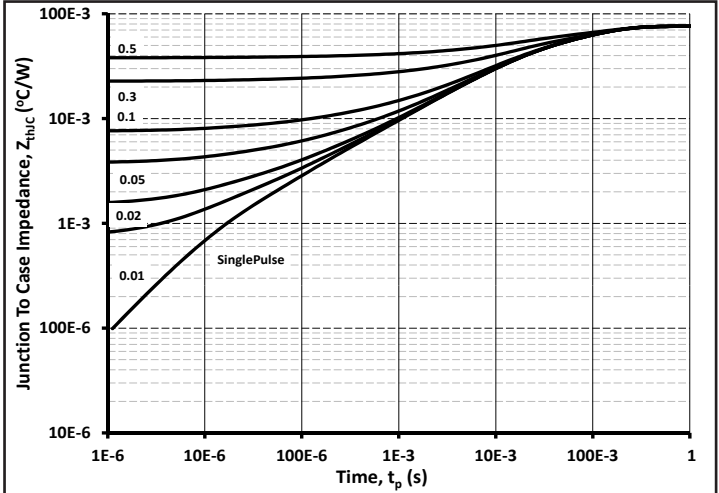
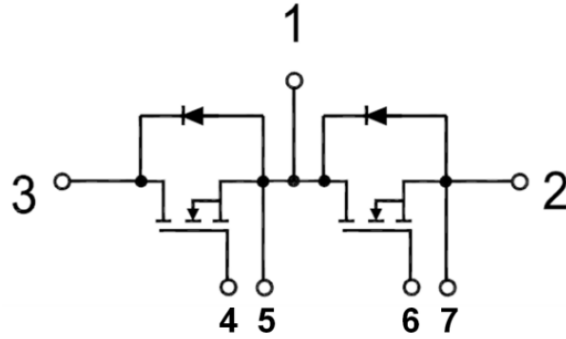
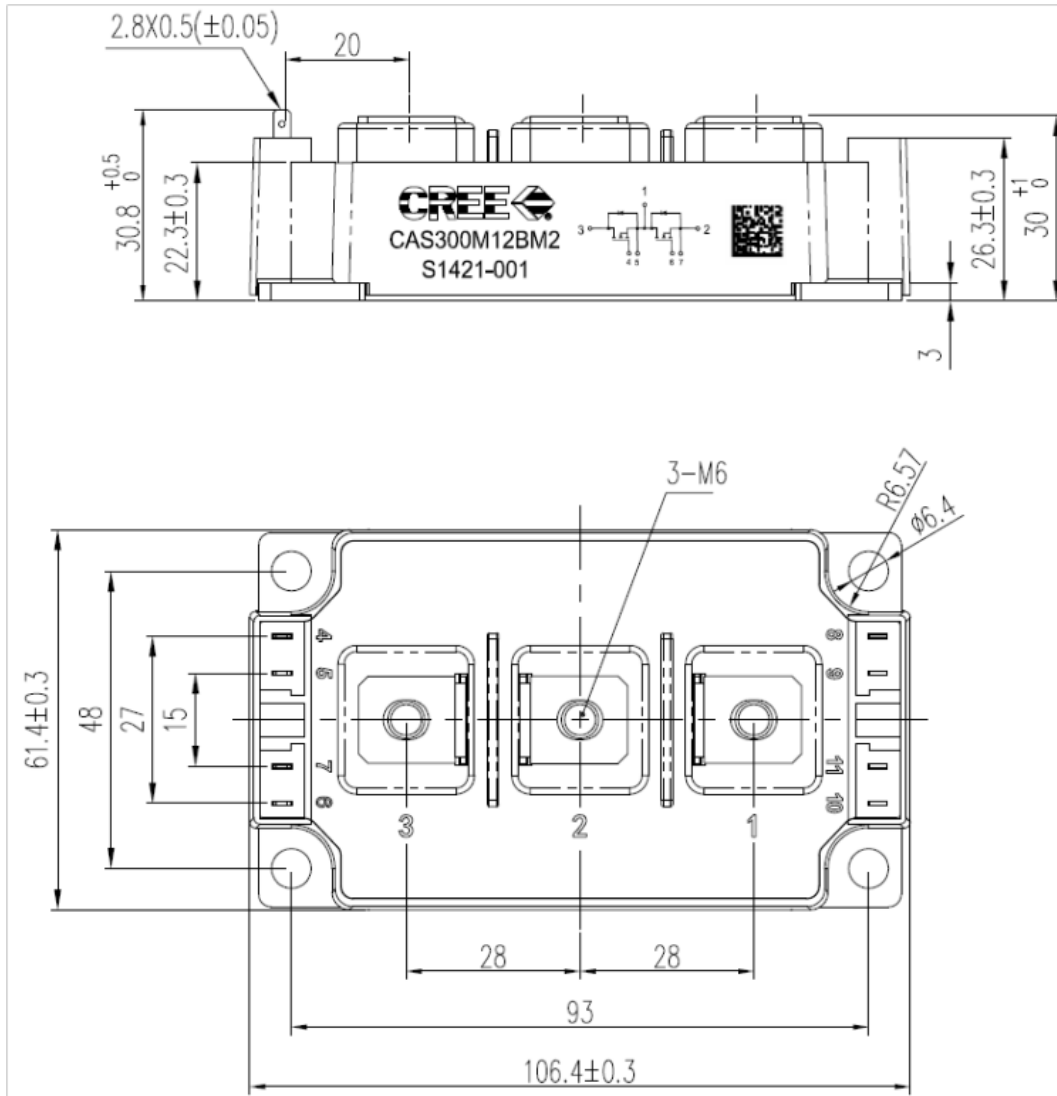


Figure 28. Diode Junction to Case Thermal Impedance

Schematic



Package Dimensions (mm)





Notes

- **RoHS Compliance**

The levels of RoHS restricted materials in this product are below the maximum concentration values (also referred to as the threshold limits) permitted for such substances, or are used in an exempted application, in accordance with EU Directive 2011/65/EC (RoHS2), as implemented January 2, 2013. RoHS Declarations for this product can be obtained from your Cree representative or from the Product Documentation sections of www.cree.com.

- **REACH Compliance**

REACH substances of high concern (SVHCs) information is available for this product. Since the European Chemical Agency (ECHA) has published notice of their intent to frequently revise the SVHC listing for the foreseeable future, please contact a Cree representative to insure you get the most up-to-date REACH SVHC Declaration. REACH banned substance information (REACH Article 67) is also available upon request.

- This product has not been designed or tested for use in, and is not intended for use in, applications implanted into the human body nor in applications in which failure of the product could lead to death, personal injury or property damage, including but not limited to equipment used in the operation of nuclear facilities, life-support machines, cardiac defibrillators or similar emergency medical equipment, aircraft navigation or communication or control systems, air traffic control systems.